PHOTODUPLICATION: 90 pp. total

vellum complete

PHOTOPRODUCTION OF NEUTRAL PIONS IN HYDROGEN FROM 600 TO 800 MEV

Thesis by

Robert M. Worlock

In Partial Fulfillment of the Requirements

For the Degree of

Doctor of Philosophy

California Institute of Technology

Pasadena, California

1958

ACKNOWLEDGMENTS

Dr. Alvin V. Tollestrup suggested this experiment; his interest and helpful suggestions during the first few months of the experiment have been invaluable as have his assistance and guidance throughout the author's graduate residence. The latter part of the experiment and the subsequent analysis have been ably supervised by Dr. Robert L. Walker, who very kindly agreed to take over these duties in Dr. Tollestrup's absence.

Dr. Arthur B. Clegg was a most useful colleague while data were being gathered and during the subsequent analysis. Dr. Ricardo Gomez was helpful in the developmental stage of the experiment. Many useful discussions were held with Dr. James I. Vette, who is also to be thanked for the development of the pair correction method used here. Mr. Marshall P. Ernstene did the majority of the coding of the telescope resolution program. Mr. Walter W. Wales coded the least squares analysis program. Mr. Earle B. Emery is to be thanked for his maintenance of the liquid hydrogen target.

The interest and encouragement throughout the author's graduate residence of Dr. Robert F. Bacher is gratefully acknowledged. The partial support of the U. S. Atomic Energy Commission is appreciated.

ABSTRACT

The photoproduction of neutral π mesons from hydrogen has been studied at the California Institute of Technology Synchrotron Laboratory by detecting recoil protons from a liquid hydrogen target irradiated by the synchrotron bremsstrahlung beam. The recoil protons were detected by a five counter telescope which comprised a standard three scintillation counter range telescope plus an additional dE/dx counter for more positive identification of the proton and a Cerenkov counter in anti-coincidence to eliminate events due to multiple electrons. The effect of recoil protons from pion pair production was reduced by lowering the bremsstrahlung endpoint energy to about 100 mev above that of the photons producing the desired events. Even so, contamination was significant at forward proton angles and correction for this effect was necessary. Data were taken at proton laboratory angles of 19°, 30°, 40°, 50°, and 60° at proton energies corresponding to photon energies of 600, 700, and 800 mev. Angular distribution data are produced at these three energies and fitted with functions of the form: $A + B \cos \theta^{*}_{\pi} + C \cos^{2}\theta^{*}_{\pi}$. These functions are qualitatively like those at lower energies; B is small and -A/C is roughly 1.25. The total cross-section is found to have a minimum at about 600 mev, being slightly larger at 700 and 800 mev.

TABLE OF CONTENTS

I. INTRODUCTION

The photoproduction of π^o mesons from hydrogen has been the subject of extensive study at this laboratory and elsewhere. Pioneering work was done by Panofsky, Steinberger, and Steller (1), who counted coincidences between the two photons produced in the π^o decay and firmly established the existence of the π^o meson and its photoproduction. Silverman and Stearns (2) counted coincidences between one decay photon and the recoil proton to obtain an excitation function in the 200-300 mev range. Goldschmidt-Clermont, Osborne, and Scott (3) counted recoil protons in nuclear emulsions to obtain angular distributions in the same energy range. At this laboratory, angular distributions have been measured in the 300-450 mev range by Walker, Oakley, and Tollestrup (4) who counted recoil proton--decay photon coincidences, and in the 260-450 mev range by Oakley and Walker (5) and McDonald, Peterson, and Corson (6) who counted recoil protons. The predominance of a single state of total angular momentum = 3/2 and isotopic spin = 3/2 in the pion-nucleon interaction and use of the scattering phase shifts from pion-nucleon scattering data in a phenomenological model have made possible a satisfactory understanding of photomeson production in the range studied (7). A meson theory calculation by Chew and Low (8) has also been successful in explaining the general features of the process in this energy region.

When a high energy photon beam became available for experimental use at the Cal Tech Synchrotron Laboratory early in 1957, it was felt that one of the first projects should be to extend our knowledge of pion photoproduction reactions into the

newly available energy range. Little theory currently exists which attempts to explain pion phenomena above about 400 mev. Comparison of photoproduction and pion-nucleon scattering which proved so rewarding at lower energies is not possible since insufficient data are presently available. It was hoped, however, that some effect in photoproduction might be found which corresponds to the peak in pion-nucleon total scattering cross-section at about 800 mev (9). In addition, high energy data should be of use in formulating pion theories in the future.

This thesis, then, describes an experiment carried out to obtain angular distributions for the photoproduction of π^o mesons from hydrogen at photon energies between 600 and 800 mev. To do this, the cross-section was measured at proton laboratory angles of 19^o, 30^o, 40^o, 50^o, and 60^o for photon energies of 600, 700 and 800 mev. To detect the desired event, a counter telescope was employed to count the recoil protons produced by the photoproduction process. At about the same time, a complementary experiment was carried on by J. I. Vette (10), using a magnetic spectrometer to detect the recoil protons. Experience at this laboratory in measuring photoproduction of π^+ mesons (11, 12) has shown that magnetic spectrometer and counter telescope experiments do not always agree as well as might be expected, so it seemed worthwhile to make overlapping measurements.

Section II begins by discussing in general terms the method used for this experiment, then proceeds to a description of the experimental equipment involved, and concludes by describing

the actual use of the equipment. Section III concerns itself with the problem of producing cross-sections from the data obtained from the experimental operation. Various corrections to the data are considered here. Section IV presents the results with their associated errors. In Section V the results of this experiment and other available data are collected together and examined for behavior of theoretical interest. Finally, in Section VI, some suggestions for more refined measurements in the future are mentioned.

II. EXPERIMENTAL TECHNIQUE

1. General Considerations

Since the π^o meson decays with a mean life of about 10^{-15} seconds into two gamma rays whose directions are not uniquely related to the π^o direction, the most convenient method for measuring the cross-section for the process $\gamma + P \rightarrow P + \pi^o$ in the energy and angular regions under consideration is to count the recoil protons rather than the mesons themselves. This method has the advantages of counting rate, simplicity, and relative ease of data reduction, but has the disadvantage that the protons counted may come from reactions other than the desired one. From hydrogen the offending reactions are:

$$\begin{aligned} \gamma + P &\longrightarrow P + \gamma' \\ &\longrightarrow P + \pi^+ + \pi^- \\ &\longrightarrow P + \pi^\circ + \pi^\circ \\ &\longrightarrow P + 3 \text{ or more mesons} \end{aligned}$$

The Compton process is improbable enough to be essentially an insignificant source of error; the multiple pion processes are much more probable, but by taking suitable precautions and making corrections based on available data, the error introduced is not excessive. These reactions will be considered more quantitatively later.

Since the gamma-ray beam produced by a synchrotron accelerating electrons to energy E_o has a continuous energy spectrum extending from zero to E_o, some method must be found for determining the energy of the photon producing a given event.

Fortunately, in reactions of the two-body type, such as the one of interest, knowledge of the energy and polar angle of the recoil proton allows one to calculate all other kinematic quantities including the pion energy and angle and the photon energy.

For counting protons, counter telescopes of the type to be described are useful in the proton energy range between about 50 and 500 mev. At the low end they are limited by the fact that the particle to be counted must enter at least two counters. At the high end they are limited by nuclear absorption, which leads to two important effects: 1) loss of counting rate and 2) error due to the uncertainty in making absorption corrections. At a range of 17 cm. of copper, corresponding to a proton energy of 460 mev, only a third of the protons incident survive to be counted, and a 1% uncertainty in the absorption cross-section produces a 1% uncertainty in the final result.

The necessity for stopping the counted proton with its associated absorption probability is probably the principal disadvantage of the telescope method in the energy range encountered in this experiment. Some other disadvantages, relative to the magnetic spectrometer method are: 1) high counting rates in the individual counters at forward angles, necessitating complicated electronics; 2) production of secondary protons in absorbers; and 3) difficulty in separating mesons from protons. Some advantages relative to magnetic spectrometers are: 1) small size and ease of handling, 2) ease of changing angular and energy resolution, and 3) absence of large scattering surfaces such as pole faces.

Thus, neither magnetic spectrometer nor telescope is definitely superior to the other for counting protons; rather, they provide a way of making independent measurements of the same thing.

Figure 1 shows a portion of the kinematics of the reaction $\gamma + P \rightarrow P + \pi^o$. Recoil proton energy is plotted against proton angle with photon energy as the parameter. Since a counter telescope counts protons in specified angular and energy ranges, a given telescope setting defines a rectangle on this diagram. The probability of being counted is not necessarily the same for protons from all points inside the rectangle if the rectangle size includes the effects of a target of finite size. The solid lines represent the single production process, $\gamma + P \rightarrow P + \pi^o$. The dotted lines represent pair production, $\gamma + P \rightarrow P + (2\pi)$ where the parenthesis mean that the two pions go off together. This case is drawn since it is the most unfavorable; that is, for a given proton energy, it is the case requiring the minimum gamma-ray energy. Thus, for synchrotron energy E_o, protons from the single process are energetically possible at all points below the $k = E_o$ line for single production and protons from the pair process are energetically possible at all points below the $k = E_o$ line for pair production. To operate without contamination by the pair process, then, the rectangle defined by the telescope must fit between the single production curve and the pair production curve for the particular machine energy chosen. It must lie above the pair curve so that no protons from the pair process

Figure 1

Proton kinematics for single and double pion photoproduction. The pair production curve is calculated for the case where the two pions go off together. The rectangle represents a typical telescope "window." The outer rectangle indicates the full width of the angular resolution, while the inner rectangle indicates the angular resolution width at half-height. 85% of the counting rate comes from the inner rectangle.

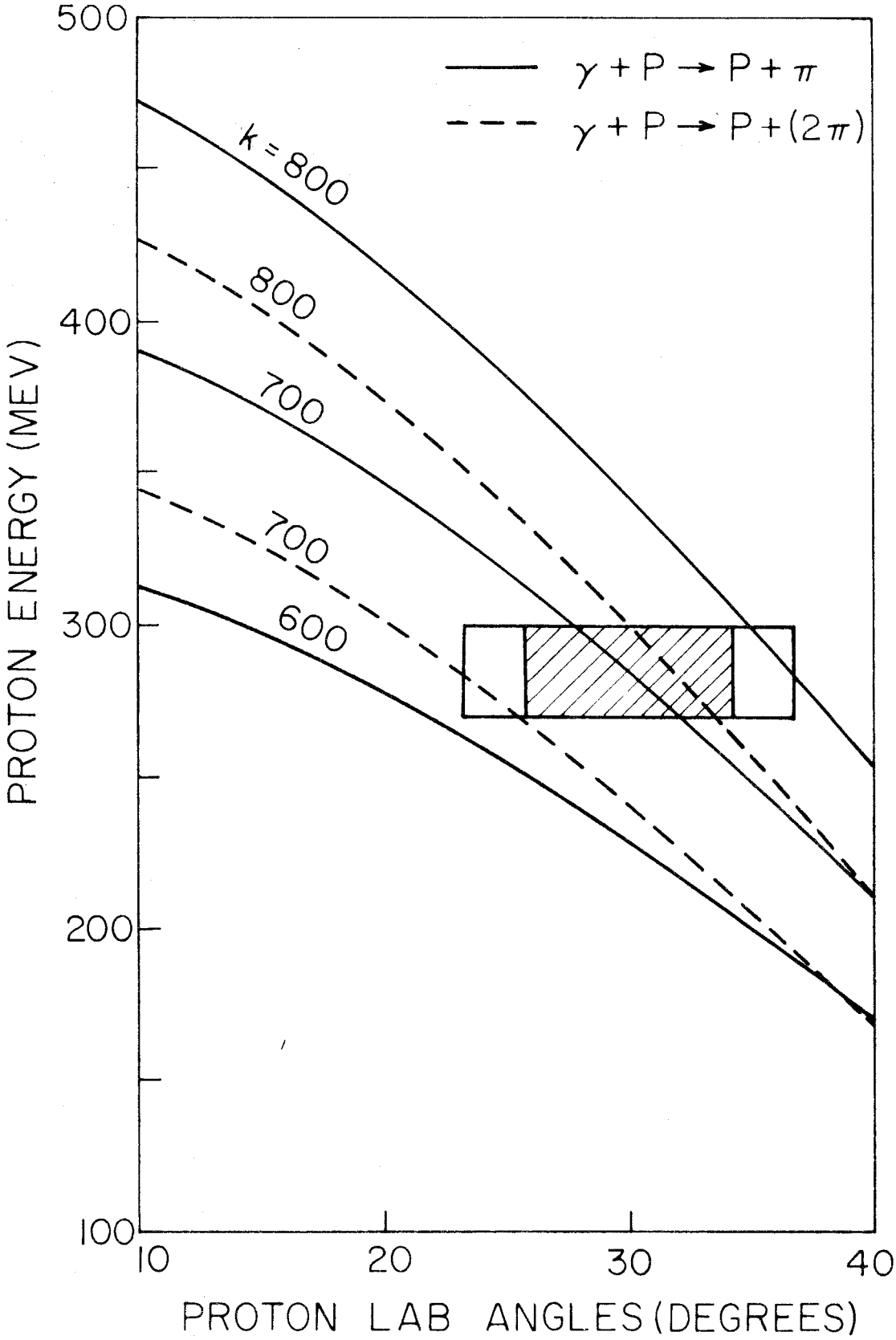
500
400
300
200
100
10
20
30
40
PROTON ENERGY (MEV)
PROTON LAB ANGLES (DEGREES)
γ + P → P + π
γ + P → P + (2π)
k = 800
800
700
700
600

can be present, and below the single production curve so that the desired protons will be present.

As can be seen from the figure, it would be very difficult to operate in this manner. Decreasing the angular and energy resolution sufficiently would make the counting rate prohibitively low. For this reason, it was decided to operate in a more conventional manner using angular resolutions of 8 to 14 degrees (full width) and proton energy resolutions of 10 to 30 mev. The machine energy or endpoint energy of the gamma-ray spectrum was determined by compromise among the various people running experiments simultaneously. It turned out to be about 120 mev above the energy being measured, which was usually enough to cover the resolution of the telescope while keeping the pair contamination down to a reasonable value. The magnitude of this contamination and correction for it will be discussed in more detail later.

2. Equipment

The telescope consisted of five counters and associated absorbers as shown in Figure 2. Counter sizes, materials, and RCA photomultiplier types are given in Table 1 below.

Table 1

Counter	Height	Width	Thickness	Material	Tube
1	3 15/64"	3"	.500"	scint. plastic	6810
2	3 1/4	2 15/64"	.490	scint. plastic	6810
3	3 1/4	2 1/2	1.002	lucite	6810
4	2 31/32	1 47/64	.235	scint. plastic	6810
4a	3	1	.250	scint. plastic	6810
5	4	3	.250	scint. plastic	6655

Figure 2

Plan view of counter telescope (schematic). Scale is 0.7 of full size. A, B, C, and D are absorbers. 1, 2, 3, 4, and 5 are counters. Protons travel in the direction of the arrow.

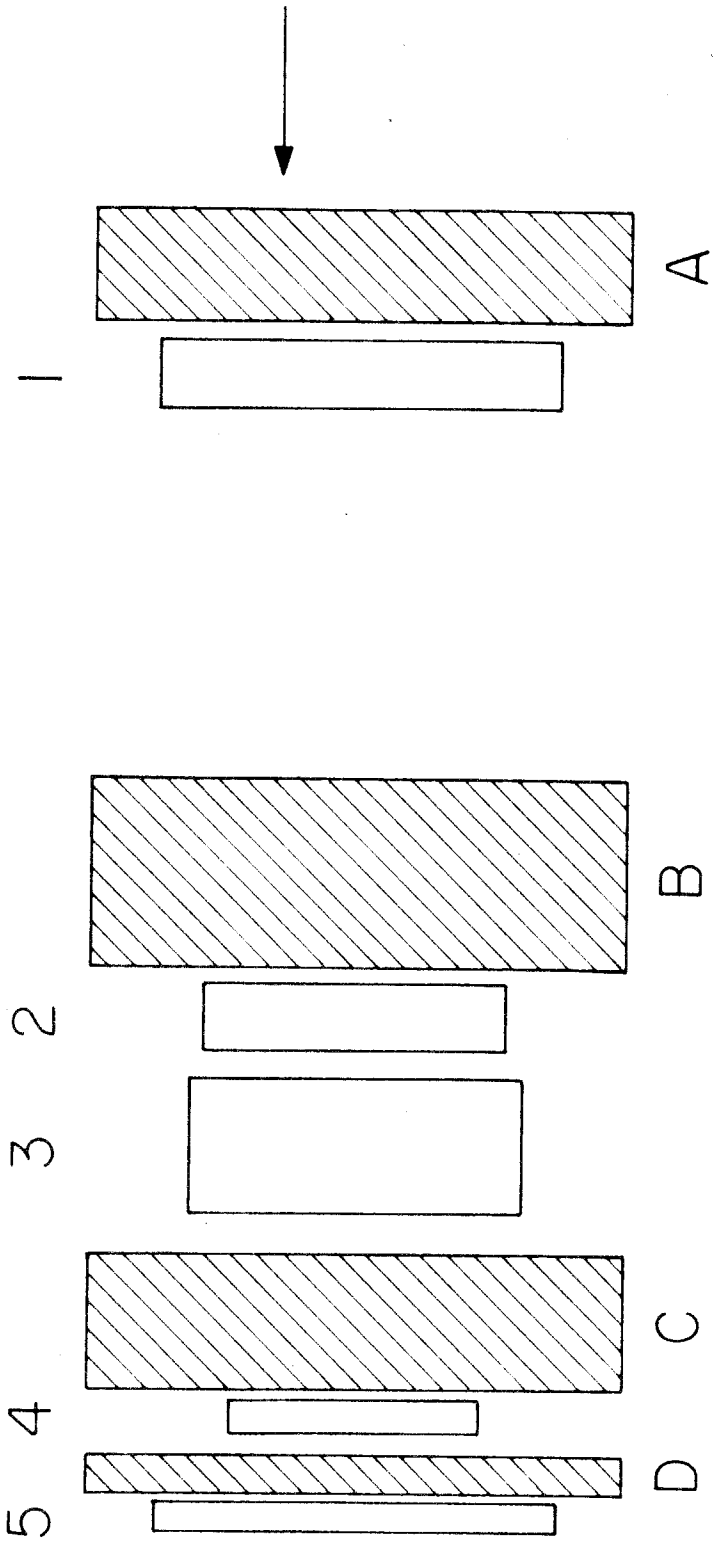
A
1
B
2
3
C
4
D
5

All counters were polished and wrapped in 6.5 mils of shiny aluminum foil. The scintillation plastic is a polystyrene base scintillator obtained from the University of California Radiation Laboratory at Livermore. Its density is 1.05 and its composition is assumed to be CH. The lucite for the Cerenkov counter is UVT type (ultraviolet transmitting), obtainable from Rohm and Haas. Its density is 1.18 and its composition is assumed to be $C_5H_8O_2$. It was chosen after some experimentation for its property of scintillating only very slightly. Standard lucite (UVA) scintillates so strongly that even when used as wall material for water filled counters, the scintillation light from slow protons is comparable to the Cerenkov light from electrons.

The dynode voltage distribution networks for counters 1 and 2, which were used for pulse height analysis, were adjusted so that the photomultipliers worked quite linearly up to 10 volt signals into 185 ohm cable.

Counters 2, 4, and 5 make up a standard three scintillation counter range telescope which operates as follows:* the range of a counted particle is determined within a certain ΔR by placing counters 2 and 4 in coincidence and counter 5 in anti-coincidence. Protons producing the proper coincidence event are identified by their specific ionization in counter 2. Counter 3, the Cerenkov counter, is sensitive to electrons and is placed in anti-coincidence to discriminate against multiple electron events which are capable

---

*For a more complete discussion of telescope operation, see Ph.D. thesis by W. R. Smythe (Cal Tech, 1957).

of producing proton-like pulses in a counter telescope. Counter 1 is placed in coincidence with a minimum of absorber in front of it. By demanding a proton-like pulse it serves two purposes: 1) It discriminates against mesons making the proper coincidence event, which, due to statistical fluctuations in energy loss in counter 2, appear to be protons, and 2) It discriminates against secondary protons made in absorber B by uncharged or lightly ionizing particles. Calculation shows that the pion and recoil neutron flux produces enough stars in absorber B with proton prongs to cause appreciable error if no precautions are taken.

Figure 3 shows a block diagram of the electronic system. Signals from counters 1, 2, 4, and 5 are fed into the Discriminator-Coincidence box, which has three coincidence and one veto channel, to form a 124(-5) coincidence output. The discrimination is done with 6BN6's and the coincidence circuit is a conventional diode type. The bias works over a 2 to 10 volt range of pulse heights and was usually used around 6 to 8. The resolving time is approximately 50 mμs and the coincidence output is a 50 mμs wide signal which opens the two-channel fast diode gate which gates the 20 mμs pulses from counters 1 and 2. The gated 1 and 2 signals are stretched in the gating circuit, amplified and sent to a slower (0.2 μs resolving time) discriminator and coincidence circuit along with the 124(-5) output signal.

Counters 2 and 3 (the Cerenkov counter) are placed in coincidence in a Garwin circuit and the output of the Garwin circuit placed in a veto channel of the slow coincidence system.

Figure 3

Simplified electronic block diagram. Amplifiers and power supplies have been left out for the sake of clarity. Synchrotron Model 522 amplifiers were used for all signals going into the slower Discriminator-Coincidence circuit. Two Hewlett-Packard Type 460B amplifiers were used after counter 5, one Type 460A was used after counter 3, and one Type 460B was used as an inverter to provide a negative signal from counter 2 to the two channel Garwin coincidence. The counter signal cables were terminated at the receiving end; no clipping was used.

Below are the Synchrotron Laboratory drawing numbers for the various circuits.

1. Two channel coincidence, Model 210: 10-T-222.
2. 50 mμs Disc.-Coinc.: 10-T-321.
3. Double Gate, Model 10: 10-T-326.
4. 0.2 μs Disc.-Coinc. (two units): 10-T-164, 165.
5. Scalers on counters 2, 4: Model 11 Scaler, 10-T-74, followed by Model 2 Scaler, 10-T-101.
6. Scalers on 124-5 and 23: Model 2 Scaler, 10-T-101.
7. Amplifier, Model 522: 10-T-163.

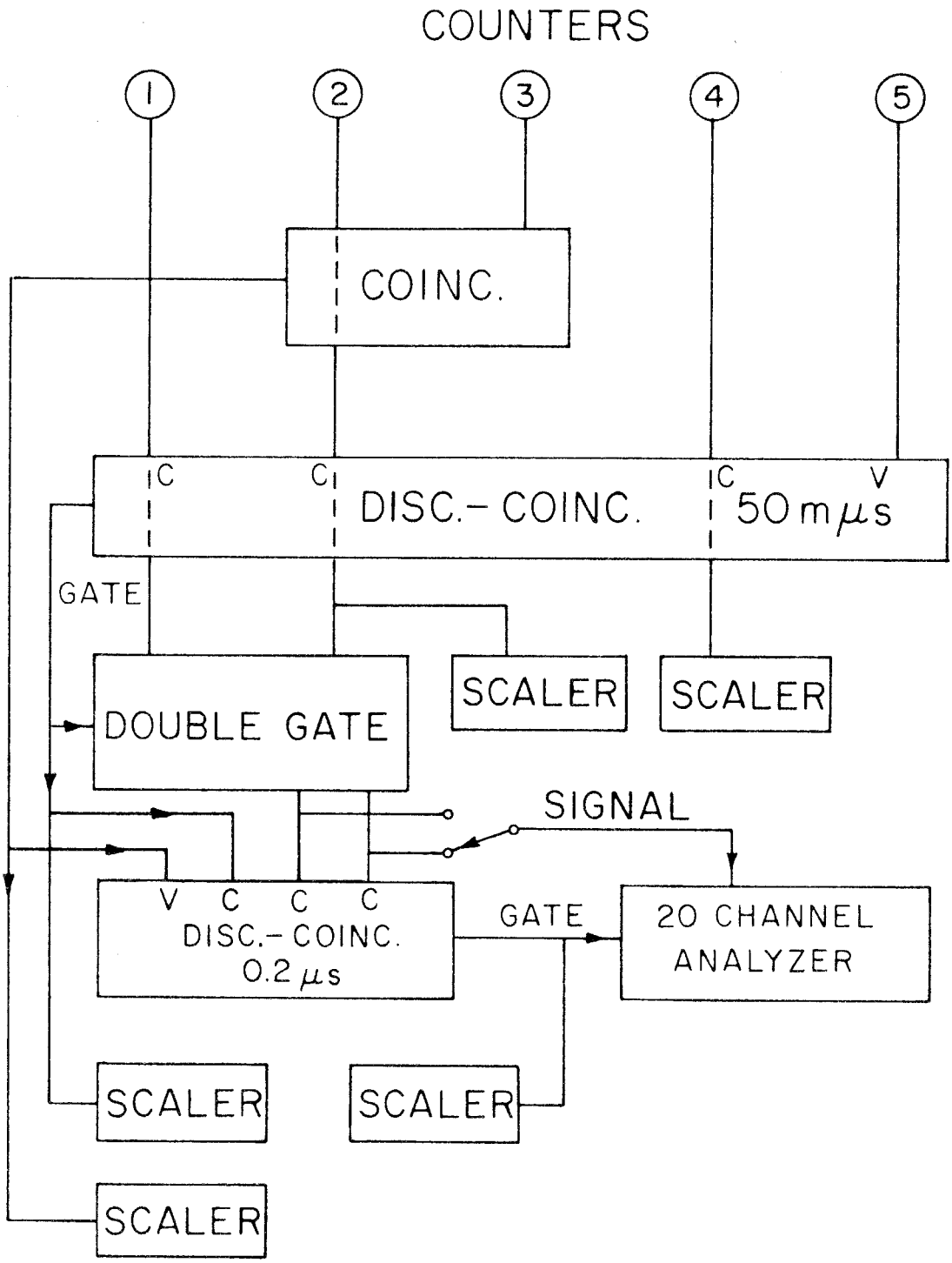

ELECTRONIC BLOCK DIAGRAM

The 23 coincidence is used rather than running counter 3 directly into a veto channel to avoid dead time losses due to 1) noise pulses from counter 3 and 2) stray counts in counter 3 due to events which didn't need to be vetoed.

The 124(-5)-(23) event as produced by the combination of the two fast coincidences and one slow coincidence circuit gates the twenty channel pulse height analyzer which then displays the pulse height from either counter 1 or 2.

Scalers monitor counters 2 and 4, 124(-5) coincidences and 23 coincidences.

The liquid hydrogen target is shown in part in Figure 4. The liquid hydrogen is contained in a mylar cup, 3" in diameter and 4" high with 3 mil walls. Provision is made to pump the hydrogen out of the cup for background runs. Surrounding the cup are thin copper and aluminum radiation shields. A 3" hole has been cut in all but one of the shields for the gamma-ray beam to pass through. Surrounding the shields is a 24 mil mylar vacuum window. A particle leaving the center of the hydrogen cup passes through 0.276 g/cm^2 of hydrogen and 0.199 g/cm^2 of radiation shields and mylar walls. The latter number is divided as follows: 0.007 g/cm^2 aluminum, 0.068 g/cm^2 copper, 0.043 g/cm^2 oxygen, 0.081 g/cm^2 carbon.

The Cal Tech synchrotron is a pulsed electron accelerator with a one per second repetition rate. Peak field corresponds to 1500 mev. When the electrons have reached the desired energy, the radio frequency accelerating voltage is decreased and the electrons gradually fall out of synchronous orbits and spiral in

Figure 4

Partial view of liquid hydrogen target.

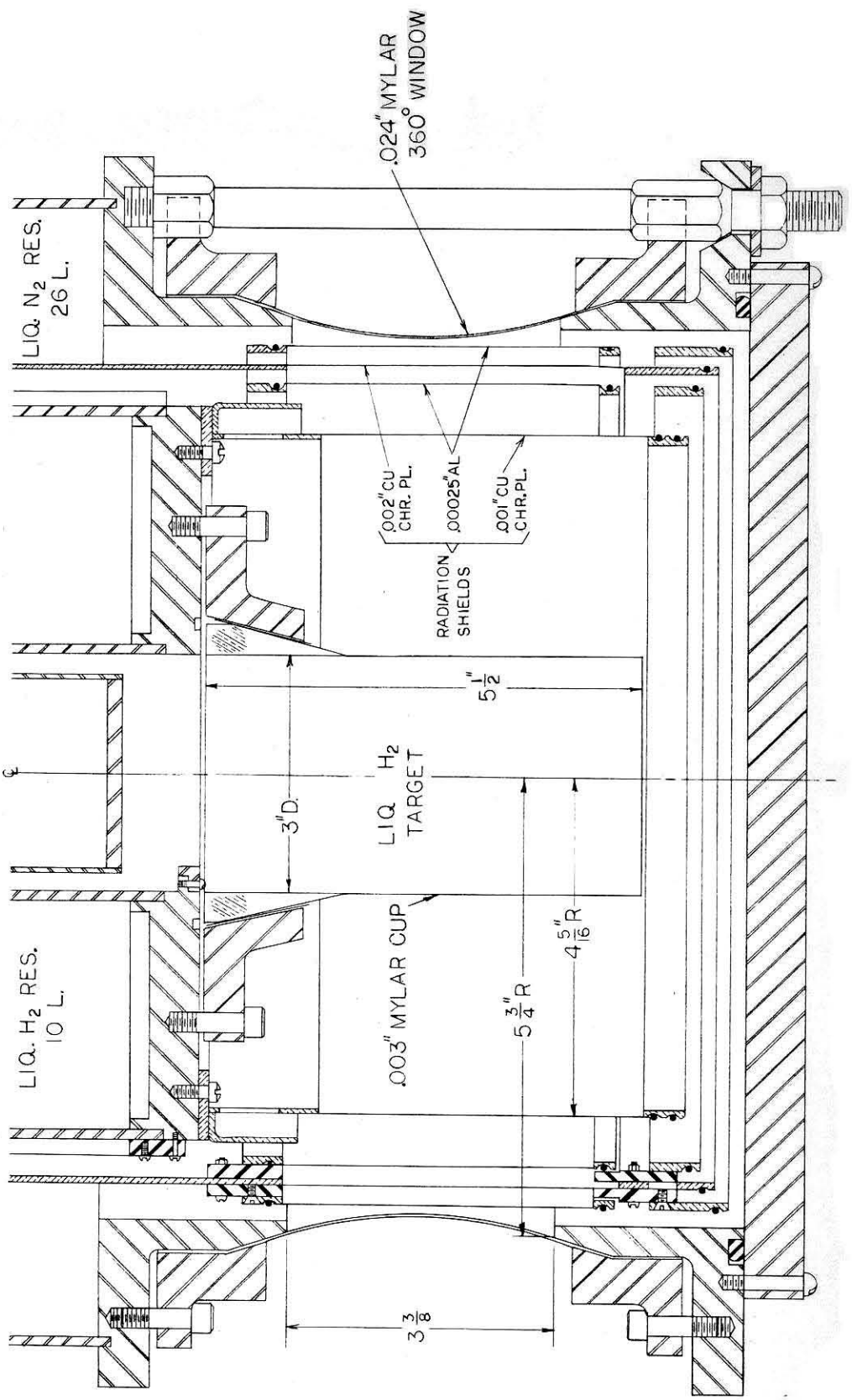
.024" MYLAR
360° WINDOW
LIQ. N_2 RES.
26 L.
.002" CU
CHR. PL.
.00025" AL
.001" CU
CHR. PL.
RADIATION
SHIELDS
$5\frac{1}{2}$"
LIQ H_2
TARGET
3" D.
LIQ. H_2 RES.
10 L.
.003" MYLAR CUP
$5\frac{3}{4}$" R
$4\frac{5}{16}$" R
$3\frac{3}{8}$

until they strike a 31 mil tantalum radiator to produce by the bremsstrahlung process a gamma-ray beam. By properly adjusting the rate of decrease of accelerating voltage the electrons can be made to hit the radiator at a more or less uniform rate for about 20 ms. During this beam time it is desirable to maintain a constant electron energy so instead of rising, the magnetic fields remain constant for the appropriate time. The electron final energy E_o is measured by integrating the signal from a pickup coil inside the machine from the beginning of the acceleration period to some time during the uniform field period covering beam dump. The value of E_o given by this coil and associated electronics agrees within 1% with that obtained from pair spectrometer measurements.

Figure 5 shows a plan view of the experimental area. The photon beam first passes through the primary collimator which is mounted in the synchrotron magnet iron. This is the only true collimation of the beam which takes place. Next in line is scraper wall No. 1, which has an aperture slightly larger than the collimated beam. Its purpose is to shield the target and nearby counters from radiation from the machine and from electrons and photons scattered off the walls of the primary collimator. It is followed by the high pressure hydrogen gas target. Here the beam passes through 60 mils of steel, 17 inches of cold, high pressure hydrogen, and a few inches of styrofoam. Next in line is scraper No. 2 which further cleans up the beam. It is followed by a series of magnetron magnets

Figure 5

Plan view of experimental area.

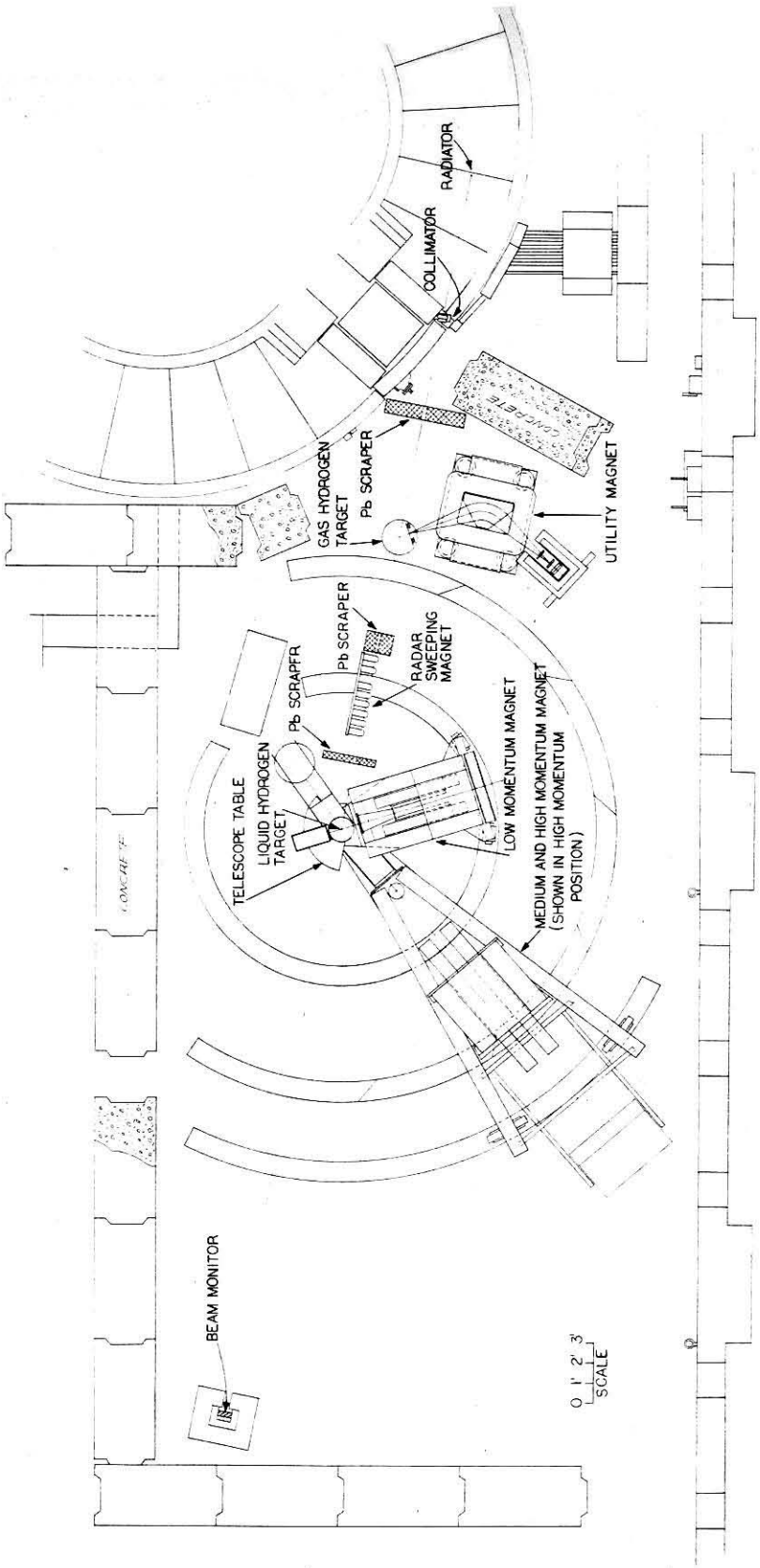
RADIATOR
COLLIMATOR
CONCRETE
GAS HYDROGEN TARGET
Pb SCRAPER
UTILITY MAGNET
Pb SCRAPER
RADAR SWEEPING MAGNET
Pb SCRAPER
LIQUID HYDROGEN TARGET
TELESCOPE TABLE
LOW MOMENTUM MAGNET
MEDIUM AND HIGH MOMENTUM MAGNET (SHOWN IN HIGH MOMENTUM POSITION)
CONCRETE
BEAM MONITOR
0 1' 2' 3'
SCALE

which serve to sweep out of the beam electron pairs which are formed in the gas target and air path as well as any other charged particles which may be in the beam. Finally, in front of the hydrogen target is scraper No. 3 which once again scrapes off any stray radiation travelling along with the beam, and further shields the target and counters.

The collimator and scraper walls are carefully lined up and checked by taking x-ray photographs to be sure that 1) the beam passes through the center of the target, 2) the primary collimator is centered on the beam, and 3) each of the scraper walls is centered on the beam and scrapes but does not collimate.

Early in the experiment the beam size at the target was approximately 6.6 cm high and 5.5 cm wide. Later the collimation and scraping system was revised slightly to produce a beam 6.0 cm high and 4.2 cm wide.

After passing through the target the beam continues about 30 feet where it strikes the beam monitor ion chamber which is set in a cavity in a large lead beam catcher block. Any beam which passes through the ion chamber is absorbed in the lead block. The lead is surrounded by paraffin blocks to reduce the neutron background in the laboratory.

The synchrotron photon beam is monitored by a Cornell-type air-filled thick-walled ion chamber, the charge from which is integrated by a Model 3 ion current integrator (Dwg. No. 10-T-217, Serial No. 0196). The unit of charge is referred to as the BIP (Beam Integrator Pulse) and the calibration of the integrator used is 2.22×10^{-7} coulomb/BIP. This calibration

was obtained using the Model 10 Integrator Calibrator (Dwg. No. 10-T-353) which discharges a precision capacitor into the integrator. The ion chamber has been calibrated by Gomez (13) by comparing it with a multiple plate ionization chamber designed by Wilson (14), the output of which is assumed to depend only on total beam energy. Using Wilson's calculated response of 4.88×10^{18} mev/coulomb, the results of Table 2 were obtained with the ion chamber in its standard position in the beam catcher.

Table 2

E_o (mev)	ion chamber mev/coulomb
497	4.45×10^{18}
789	5.05
1080	5.41

Defining U ≡ mev/BIP and E_o ≡ bremsstrahlung upper limit, the number of photons/BIP at energy k in an interval dk is $N(k) \equiv U/E_o\, B(k, E_o)\, dk/k$. $B(k, E_o)$ contains the deviations in the spectrum from a 1/k dependence and is normalized so that $\int_o^{E_o} B(k, E_o)dk \equiv 1$. On the basis of pair spectrometer measurements by Donoho, Emery, and Walker (15), $B(k, E_o)$ is assumed constant with a value 0.90 for values of k/E_o between 0.6 and 1.0. This is a simple approximation to the theoretical thin target spectrum and gives results indistinguishable from the latter for an experiment with an energy resolution as poor as the present one. The pair spectrometer measurements were of limited accuracy because of a troublesome background, but showed that the spectrum was much closer to that expected for a thin target than to that expected from a target of the nominal thickness (0.2 radiation lengths) of the one in the

synchrotron. Presumably the electrons spiral in so slowly that they barely graze the edge of the target.

The beam intensity distribution over the target was measured by J. I. Vette (10) by exposing in the beam electron sensitive nuclear emulsion plates whose positions relative to the target cylinder were known. After development, measurements were made with a densitometer and a beam intensity distribution function determined using the following coordinates: origin at center of target, z along beam direction, x vertical, and y chosen to form a right handed orthogonal system. The function, called $n(\tilde{r})$, is assumed to be symmetrical about some line parallel to the z axis and independent of z. It is normalized so that $\iint n(\tilde{r})\, dx\, dy = 1$. The role of this function in the calculation of cross-sections is discussed in Section III and Appendix A.

3. Operation

The first step in putting the counter telescope into operation was timing the gates and coincidence circuits. This was first done roughly using an oscilloscope. The scope was triggered from some convenient counter and the various cable lengths adjusted until the inputs to any given circuit arrived at suitable times. To check this setting, delay curves were run on the coincidence circuits and final adjustments made.

Having determined that the electronic equipment was working, the next step was to use the telescope as a unit to count protons. Having chosen a proton angle and energy there remains a number of choices and adjustments to be made. The proton energy

determines the range (16). Absorbers A, B, C, and D were then chosen as follows: Absorber D was arrived at by a compromise between high counting rate (counting rate varies linearly with D) and good energy resolution. Absorber C was chosen to give close to optimum separation of meson and proton peaks as seen in counter 2. Absorber A was a low-z material such as CH_2 or aluminum to minimize scattering and secondary proton production; only enough was used to keep the counting rate in counter 1 down to a reasonable figure. Last of all, absorber B was chosen to bring the total mean range up to the desired value. Copper blocks, 4" square, were used for absorbers B, C, and D.

For a given set of absorbers, the photomultiplier and amplifier gains next had to be set. Counters 4 and 5 were permanently set to give about 6 volt pulses at the Discriminator-Coincidence input from Co^{60}. The bias was then set to count everything over 3 volts. It is desirable to have high gain and low bias (consistent with keeping counting rates reasonable) on these two counters so that particles do not have to penetrate the counters very far in order to be counted. Under these circumstances, ΔR, which is involved directly in the counting rate, can be calculated quite accurately from knowledge of the material in the telescope and is insensitive to small drifts in counter gains. Assuming that counters 4 and 5 are made of the same material, gains and biasses should be set so that the same Co^{60} signal just triggers both counters. Then the distance that a stopping proton must penetrate to be counted cancels out of the expression for ΔR. This is advantageous since plastic scintillators exhibit strong saturation effects and this

distance is not easily calculable.

The photomultiplier gains on counters 1 and 2 were set so that proton pulses were 6 to 8 volts, a region where the bias circuit worked well. The photomultiplier gain on counter 3 was set on a plateau for counting electrons. This was done by putting counter 3 in coincidence (requiring 124(-5)23) and counting electron pulses in counter 2.

It was noticed that the UVT lucite scintillates slightly, although much less than the ordinary UVA lucite. By operating at a large angle where electron contamination was unimportant and observing the proton peak in counter 2, comparison of 124(-5) runs with 124(-5)23 runs yielded the fraction of protons counted by counter 3 as a function of counter 3 gain and proton energy loss in counter 3. The results of this and the electron counting experiments are shown in Figure 6. For the proton energies encountered in the experiment, the error due to vetoing protons was less than 1%.

Having chosen absorbers and photomultiplier gains, only the biasses on counters 1, 2, 4, and 5 remained. As explained previously, the biasses on 4 and 5 were permanently set to count at about 0.5 mev loss in the scintillator as determined by Co^{60}. To set biasses 1 and 2 the procedure was as follows: Set both biasses low and display counter 1 on the pulse height analyzer. Set bias 1 slightly below the bottom of the proton peak. Then display counter 2 on the pulse height analyzer and set bias 2 similarly. Counter 2 was displayed during actual data taking since the

Figure 6

Efficiency of Cerenkov counter for counting electrons and protons as a function of photomultiplier voltage. Different proton curves are for different amounts of energy lost by protons in 1" of lucite.

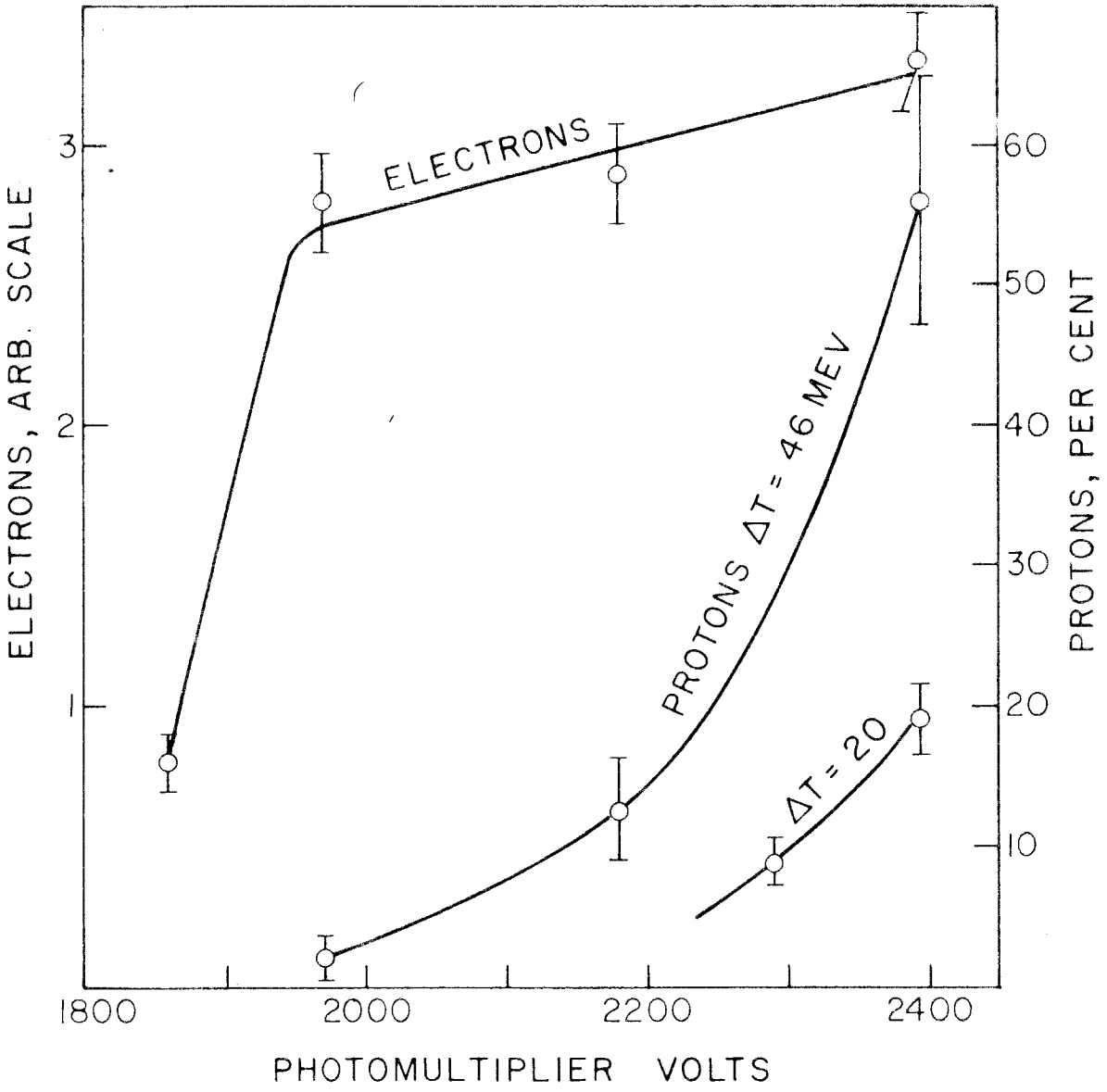
ELECTRONS
PROTONS ΔT = 46 MEV
ΔT = 20
ELECTRONS, ARB. SCALE
PROTONS, PER CENT
PHOTOMULTIPLIER VOLTS
1800
2000
2200
2400
1
2
3
10
20
30
40
50
60

peaks there were easier to separate than in counter 1. The bias settings had to be checked at frequent intervals since they and the photomultiplier gains drifted slightly from time to time.

As a check on the apparatus and calculation of ΔR, a "ΔR curve" was run*. Assuming a uniform or linear proton energy spectrum, counting rate is proportional to ΔR, which consists approximately of the material between the front of counter 4 and the front of counter 5. A ΔR curve is run by counting protons for a given number of BIPs as a function of absorber D, adjusting absorber B so that the mean range is kept constant. These data are fitted with a straight line and the intercept at zero counting rate identified as the contribution of the counters to ΔR in terms of the absorber material used. A couple of determinations of this type were made and gave satisfactory agreement with calculations.

A typical pulse height spectrum from counter 2 as recorded by the pulse height analyzer is shown in Figure 7. It was obtained at a proton angle of 30° and proton energy of 332 mev. The absence of the meson peak is due to the high bias settings on counters 1 and 2. About a third of the width can be ascribed to the proton energy range acceptable by the telescope; the rest is due to the resolution of the counter. At larger proton angles, the peak to valley ratio was slightly better and at smaller angles it was somewhat worse.

Data were taken with and without hydrogen in the target at proton energies corresponding to photon energies of 600, 700, and

---

*See Ph. D. thesis by W. R. Smythe (Cal Tech, 1957).

Figure 7

Proton pulse height spectrum. Proton energy is 332 mev, proton laboratory angle is 30^{o}.

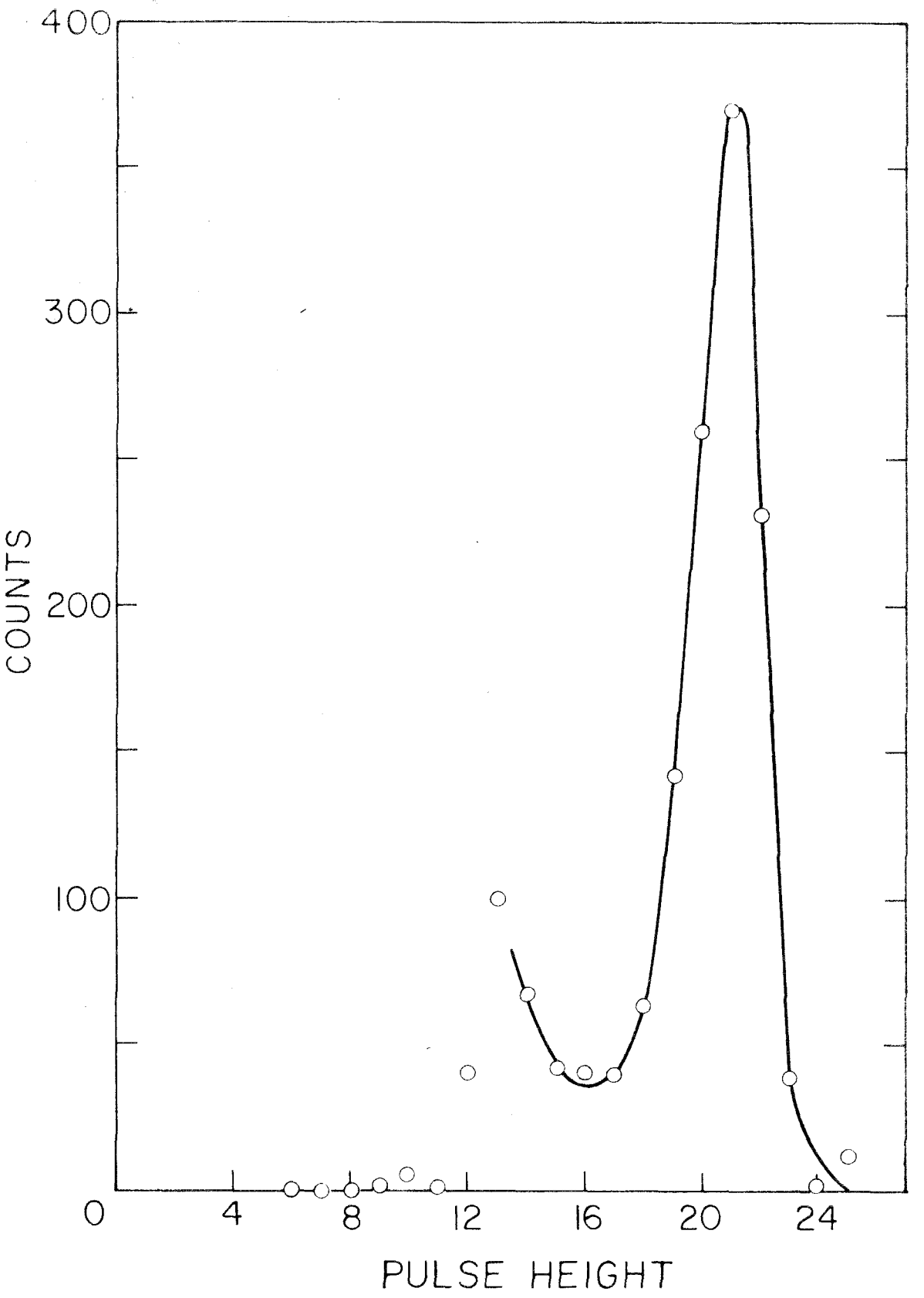
400
300
200
100
0
COUNTS
4
8
12
16
20
24
PULSE HEIGHT

800 mev and proton lab angles of 19°, 30°, 40°, 50°, and 60°. Run lengths were divided between full target and empty target to give minimum statistical errors for a given total number of BIPs. At 19°, 30°, and 40°, enough data were taken to give approximately 5% statistics; at 50° and 60°, 7% statistics were obtained. The machine energy E_o and the ion chamber pressure and temperature were monitored so that all runs could be corrected to STP and corrected for variations in E_o from run to run.

The ratio of empty target counting rate to full target counting rate varied between 15% and 50%, with the higher values occurring at the forward proton angles. At proton angles of 50° and 60°, it was possible to erect lead walls which prevented protons produced in the mylar vacuum window from being counted.

To maintain the contributing photon energy interval at a reasonable value, the energy and angular resolution of the telescope had to be changed as a function of angle and energy. The angular resolution, produced both by the width of the defining counter in the telescope and by the finite size of the target was changed by varying the distance from the target to the defining counter and by using different defining counters, one 1 3/4" wide and one 1" wide. The proton energy resolution was changed by varying ΔR as described earlier.

Tables 3 and 4 indicate for each point the following quantities: distance from target center to defining counter, width of defining counter, full target and empty target counting rates, nominal machine energy, range, ΔR, absorbers A, B, C, and D.

Table 3

Column 1: Point number.

Column 2: Proton laboratory angle, degrees.

Column 3: Mean photon energy, mev.

Column 4: Range, cm. of copper.

Columns 5 - 8: Absorbers A, B, C, and D in cm. of copper unless otherwise specified. Density of Al is 2.70, density of CH_2 is 0.915, density of copper is 8.95.

Column 9: ΔR, cm. of copper.

Table 3

No.	θ_p	k	R	A	B	C	D	ΔR
1	19	599	7.624	1.563	1.820	2.460	1.198	1.317
2	21	613	7.624	1.563	1.820	2.460	1.198	1.317
3	19	702	11.15	5.00 Al	5.156	2.460	1.198	1.317
4	19	804	15.00	5.00 Al	8.996	2.460	1.198	1.317
5	30	600	5.429	$2.50\,Al\,CH_2^{1.29}$	1.641	1.198	.622	.743
6	30	709	8.097	5.00 Al	2.096	2.460	1.198	1.317
7	30	765	9.640	5.00 Al	3.629	2.460	1.198	1.317
8	30	793	10.38	5.00 Al	4.378	2.460	1.198	1.317
9	40	601	3.318	1.29 CH_2	.565	1.198	.327	.449
10	40	699	4.782	1.19 Al	.327	2.460	.782	.903
11	40	795	6.394	2.50 Al	1.474	2.460	.782	.903
12	50	600	1.627	1.29 CH_2	0	.116	.238	.361
13	50	693	2.337	1.29 CH_2	0	.782	.327	.449
14	50	800	3.206	1.29 CH_2	.443	1.198	.327	.449
15	60	600	.562**	0	0	.116	.038	.168
16	60	700	.846*	0	0	.160	.038	.168
17	60	803	1.183*	1.29 CH_2	0	.276	.078	.209
18-20	19	402	2.637	1.19 Al	0	.782	.487	.609
21-23	30	425	2.182	1.19 Al	0	.327	.487	.609

* Counters 1 and 3 removed

** Counter 3 removed

Table 4

Column 1: Point number.

Column 2: Proton laboratory angle, degrees.

Column 3: Mean photon energy, mev.

Column 4: Distance from target center to defining counter (#4), cm.

Column 5: Width of defining counter, cm.

Column 6: Nominal machine energy, mev.

Column 7: Full target counting rate; counts per BIP corrected to STP and for variations in E_o.

Column 8: Empty target counting rate; counts per BIP corrected to STP and for variations in E_o.

Table 4

No.	θ_p	k	L	W	E_o	C_1	C_2
1	19	599	50.4	2.20	712	7.65	3.92
2	21	613	50.4	2.20	730	7.29	3.71
3	19	702	50.4	2.20	830	4.00	1.74
4	19	804	50.4	2.20	938	2.16	0.60
5	30	600	50.4	2.20	720	6.44	2.84
6	30	709	50.4	2.20	826	5.76	1.73
7	30	765	50.4	2.20	820	3.62	1.07
8	30	793	50.4	2.20	904	3.24	0.90
9	40	601	50.4	2.20	714	5.00	2.17
10	40	699	66.6	2.20	830	4.47	1.85
11	40	795	66.6	2.20	942	2.64	1.12
12	50	600	68.0	1.27	728	1.30	0.25
13	50	693	68.0	1.27	828	1.36	0.21
14	50	800	68.0	1.27	905	0.82	0.11
15	60	600	68.0	1.27	718	1.13	0.37
16	60	700	68.0	1.27	826	0.710	0.195
17	60	803	68.0	1.27	905	0.553	0.177
18	19	402	50.4	2.20	710	35.1	12.9
19	19	402	50.4	2.20	904	37.1	10.7
20	19	402	50.4	2.20	1098	37.6	13.0
21	30	425	50.4	2.20	820	34.2	7.7
22	30	425	50.4	2.20	957	34.1	8.6
23	30	425	50.4	2.20	1085	34.5	9.1

III. DATA REDUCTION

1. Corrections

The result of the telescope operation is a set of proton counting rates: counts/BIP as a function of proton energy and angle. The first step in the data reduction is to apply to these raw data corrections for various effects which cause differences from the "true" counting rate. These corrections, which will be discussed below, are: 1) Absorption, 2) Pion pair process contamination, 3) Compton process, 4) Scattering, and 5) Electronic.

The correction for absorption of protons in the absorbers and counters was calculated (assuming the entire proton path to be in copper) from the results of Fernbach, Serber and Taylor (17), who considered the problem of scattering of a neutron wave by a sphere of material characterized by an absorption coefficient and an index of refraction. Since absorption is due to nuclear rather than electromagnetic interactions, charge independence may be invoked and their results applied to protons.

The absorption coefficient for a particle in nuclear matter is

$$K = \frac{A}{\frac{4}{3}\pi R^3}\sigma$$

where A is the number of nucleons per nucleus, σ is the scattering cross-section per nucleon for the proton, and R is the nuclear radius. The absorption cross-section for the sphere is then:

$$\sigma_a = \pi R^2 \left\{ 1 - \left[1 - (1+2KR)e^{-2KR} \right] \frac{1}{2K^2R^2} \right\}$$

σ must be the appropriately weighted average of σ_{pp} and σ_{np} and is given by

$$\sigma = \frac{1}{A}\left[Z\sigma_{pp} + (A-Z)\sigma_{np}\right]$$

The correction to the free nucleon np and pp cross-sections due to the presence of the target nucleon in a nucleus has been calculated by Goldberger (18) using the statistical gas model of the nucleus. The corrected cross-sections are smaller since the exclusion principle demands that, in the final state, both the incident and target nucleon be outside the occupied sphere in momentum space. The result is:

$$\sigma = \left[1 - \frac{1.4\,E_f}{E+V}\right]\sigma_{free}$$

where E_f = Fermi energy, E = kinetic energy of the incident particle, and V = nuclear well depth. Combining results,

$$\sigma = \left[1 - \frac{1.4E_f}{E+V}\right]\frac{1}{A}\left[Z\sigma_{pp} + (A-Z)\sigma_{np}\right]$$

where σ_{pp} and σ_{np} are now the free nucleon cross-sections. The absorption cross-section for copper was calculated as a function of energy using $E_f = 25$ mev, $V = 30$ mev, $R = 1.37 \times 10^{-13} A^{1/3}$, and the np and pp cross-sections quoted by Rossi (19). These cross-sections are consistent with the measured values quoted by Millburn, et al (20). The calculated cross-section was integrated to obtain the function $F(r)$, the fraction of protons of range r that come to rest in copper without being absorbed.

$$F(r) = \frac{N}{N_o} = \exp\left[-\int_0^r \sigma_a(x)\,\rho\frac{N_o}{A}\,dx\right]$$

Since the absorption of a proton after being counted in counter 4 causes no error, the correction factor applied to the measured counting rate is:

$$F\left(\frac{\Delta R}{2}\right) \Big/ F(R)$$

Our knowledge of the pion pair process at the present is rather fragmentary, due both to lack of any high energy pion theory and the difficulty of obtaining experimental data on three-body reactions. However, the results of M. Bloch (21) for the process $\gamma + P \rightarrow P + \pi^+ + \pi^-$ provide a basis for calculating a correction to the data of this experiment. Bloch obtained π^- energy spectra at two angles for four values of E_o, the bremsstrahlung upper limit. By subtraction, these data yield the cross-section $d^2\sigma/dT_\pi - d\Omega'$ at three energies for each of the two angles. Integrating over the π^- energy gives $d\sigma/d\Omega'$ which, within the statistics, is isotropic in the cm system and is a constant function of k between 660 and 1000 mev. Multiplying by 4π gives a total cross-section of 5×10^{-29} cm^2 with about 25% statistical error.

The desired information, for purposes of making the correction, is the proton energy spectrum as a function of angle and machine energy. Since so little is known about the interaction one must begin by making assumptions and determine later the reasonableness of the assumptions. The assumptions in this calculation are: 1) The proton angular distribution is isotropic in the cm system, and 2) The matrix element for the photoproduction process is independent of proton energy so that the proton energy spectrum is proportional to $g(k, E')$, the phase-space factor, where

E' = proton cm energy.

Using the total cross-section σ_{TP} of Bloch, the total number of pairs formed per BIP by photons of energy k in Δk is:

$$\frac{dN}{dk}\Delta k = \sigma_{TP}\frac{U}{E_o}\frac{B(k,E_o)}{k}\Delta k\,\frac{\rho N_o \bar{\ell}}{A}. \qquad \left(\frac{\rho N_o \bar{\ell}}{A} = \text{target protons/cm}^2\right)$$

Then, using the above assumptions, the proton spectrum, integrated over angles, formed by the same k in Δk is:

$$\frac{d^2N}{dE'dk}\Delta k = \sigma_{TP}\frac{U}{E_o}\frac{B(k,E_o)}{k}\Delta k\,\frac{\rho N_o \bar{\ell}}{A}\,\frac{g(k,E')}{G(k)}$$

where $G(k) = \int g(k,E')dE'$

The total proton spectrum for a machine energy of E_o is then:

$$\frac{dN}{dE'} = \sigma_{TP}\frac{U}{E_o}\frac{\rho N_o \bar{\ell}}{A}\int_o^{E_o} dk\,\frac{B(k,E_o)}{k}\,\frac{g(k,E')}{G(k)}$$

If a telescope accepts protons of energy E_{min} to E_{max} emitted into $\Delta\Omega$, the counting rate per BIP due to $\gamma + P \rightarrow P + \pi^+ + \pi^-$ according to this model is then, assuming σ_{TP} constant and neglecting the variation of the integrand over $\Delta\Omega$:

$$\frac{N_p}{BIP} = \sigma_{TP}\frac{U}{E_o}\frac{\rho N_o \bar{\ell}}{A}\frac{\Delta\Omega}{4\pi}\int_o^{E_o} dk \int_{E_{min}}^{E_{max}} dE\,\frac{d\Omega'}{d\Omega}\,\frac{B(k,E_o)}{k}\,\frac{g(k,E')}{G(k)}\,\frac{dE'}{dE}$$

Sam Berman has obtained an expression for $g(k, E')$ by integrating out all the meson variables in the density of states for a three particle final state. Using this expression, J. I. Vette and R. L. Walker have developed a code to enable the Datatron digital computer to evaluate the following integral:

$$Y = \int dk \int dE \; \frac{d\Omega'}{d\Omega} \; \frac{B(k,E_o)}{k} \; \frac{g(k,E')}{G(k)} \; \frac{dE'}{dE}$$

$$\text{Then } \frac{N_p}{BIP} = \sigma_{TP} \; \frac{U}{E_o} \; \frac{\rho N_o \bar{l}}{A} \; \frac{\Delta\Omega}{4\pi} \; Y\left(E_{min}, E_{max}, E_o, \theta_p\right)$$

The process $\gamma + P \rightarrow P + 2\pi^o$ also produces recoil protons and must be taken into account. No experimental data exist for this process, so the same assumptions are made as for the (π^+, π^-) process. Thus, to take the (π^o, π^o) process into account, σ_{TP} above is replaced by $\sigma_{TP}(1 + a)$ where a is a constant which must be determined experimentally.

To check the model described above and determine a value for a, a series of measurements was made to determine the effect of pair production on proton counting rates. This was done by setting the telescope for a given energy and angle and making runs with different values of E_o, the machine energy. By making these runs consecutively, any drifts in apparatus were eliminated as much as possible. The same procedure was followed somewhat later for the empty target runs. Experimental data for these measurements are listed under Nos. 18 to 23 in Tables 3 and 4. Figures 8 and 9 show the results converted into cross-sections with and without the pair correction as calculated above. The cross-sections at $E_o = 500$ mev are due to Oakley and Walker (5). An approximate energy dependence of σ_{TP} was included in the correction; σ_{TP} was assumed to rise linearly from zero at $k = 500$ mev to 5×10^{-29} cm^2 at $k = 600$ mev, at which point it levelled off and

Figures 8 and 9

Results of measurements made to determine the effect of pion pair production on proton counting rates. Different sets of points correspond to different values of the parameter a. Since the correction is proportional to (1 + a), a = -1 is used to label the uncorrected data.

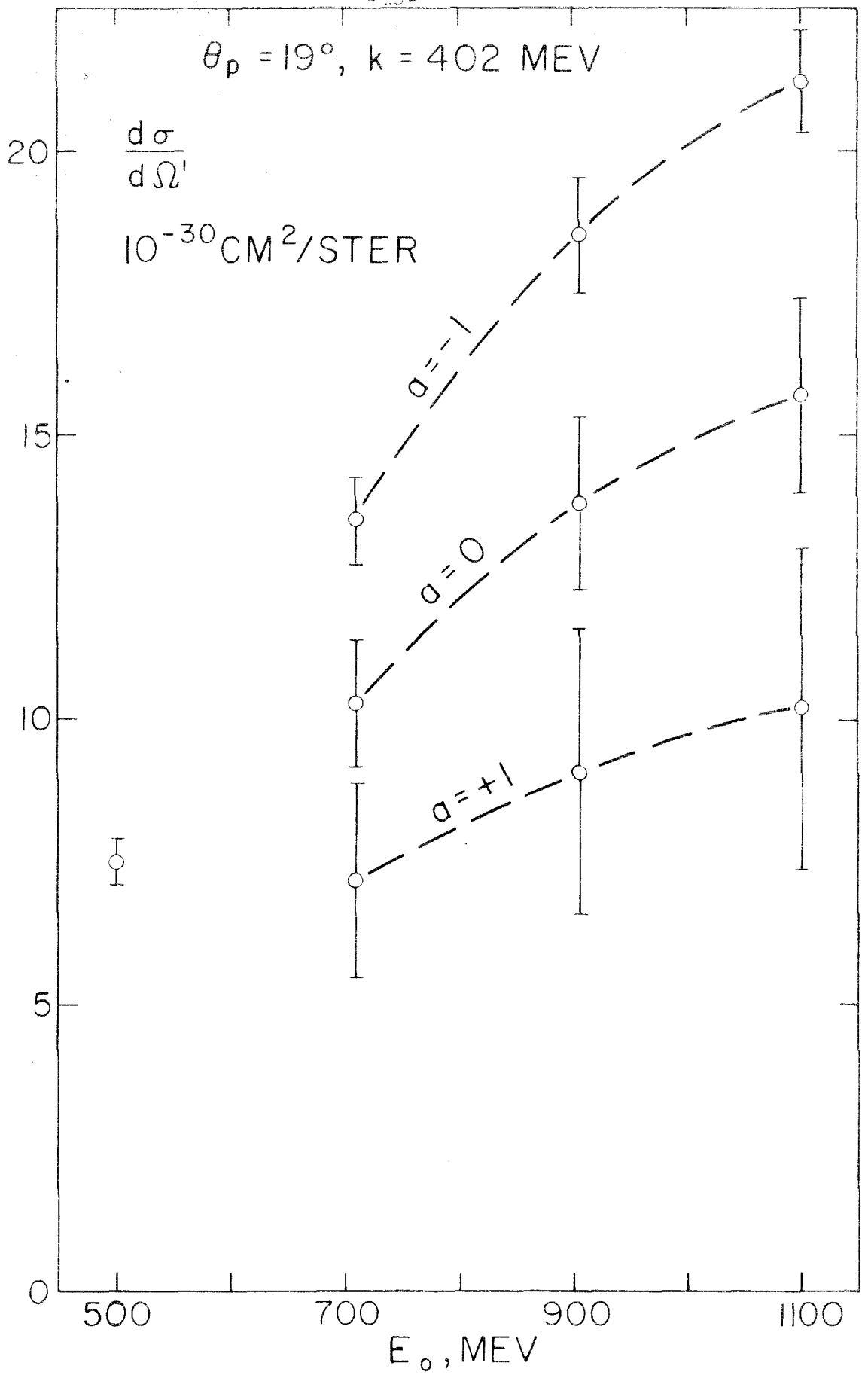
θ_p = 19°, k = 402 MEV
$\frac{d\sigma}{d\Omega'}$
10^{-30} CM^2/STER
a = -1
a = 0
a = +1
20
15
10
5
0
500
700
900
1100
E_o, MEV

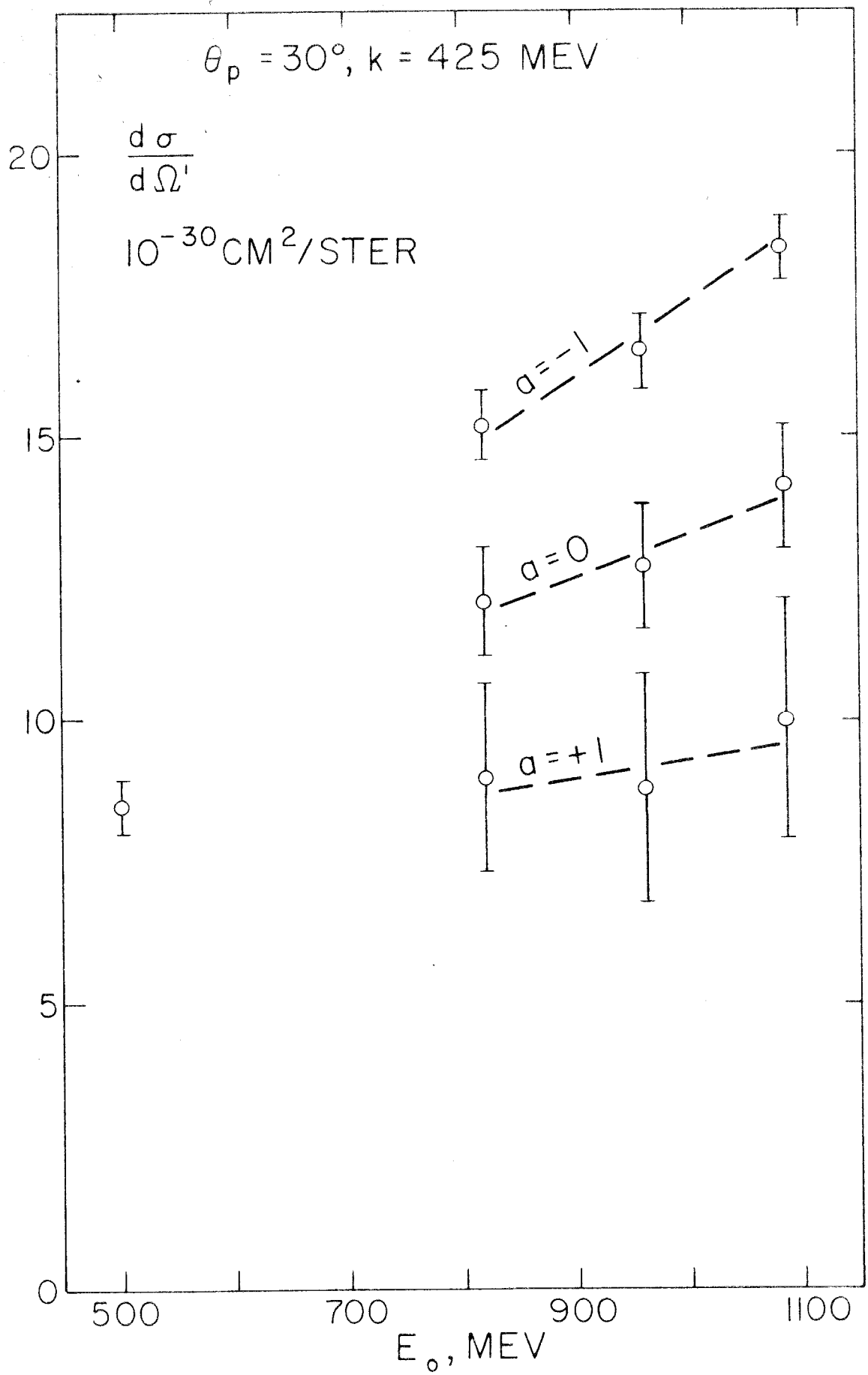
$\theta_p = 30°$, k = 425 MEV
$\frac{d\sigma}{d\Omega'}$
10^{-30} CM^2/STER
a = -1
a = 0
a = +1
20
15
10
5
0
500
700
900
1100
E_o, MEV

remained constant.

On the basis of these measurements, it was decided that a = 1 should be used in making corrections to the data. This is in disagreement with Vette (10), who concluded that a = 0 should be used.

Figure 10 shows the similarity between the kinematics of Compton scattering and single pion photoproduction. Measurements of the Compton scattering cross-section made up to photon energies of 270 mev indicate that it is about 1% of the π^o photoproduction cross-section at the same energy (22). A calculation of the Compton cross-section by Mathews (23) in the same region based on dispersion theory indicates a relationship between Compton scattering and π^o photoproduction. For this reason it is considered unlikely that the Compton cross-section exceeds a few per cent of the π^o cross-section in the region under consideration in this experiment and no correction has been made.

Scattering corrections in this experiment are just small enough to be disregarded. The following effects have been considered and found to produce errors somewhat less than a per cent in the most unfavorable case: 1) Lateral "wander" of particles in copper absorber stack, and 2) Scattering in absorbers A and B. These effects produce error due mainly to the finite size of the absorber blocks and are therefore more important in the vertical direction, where the size of the defining counter is nearly that of the absorber blocks.

At the lowest proton energy, the rms scattering angle of a particle leaving the target is about 1^o. This must be included

Figure 10

Recoil proton kinematics for the reactions $\gamma + P \rightarrow P + \pi^o$ and $\gamma + P \rightarrow P + \gamma'$ for photon energies of 600 to 800 mev.

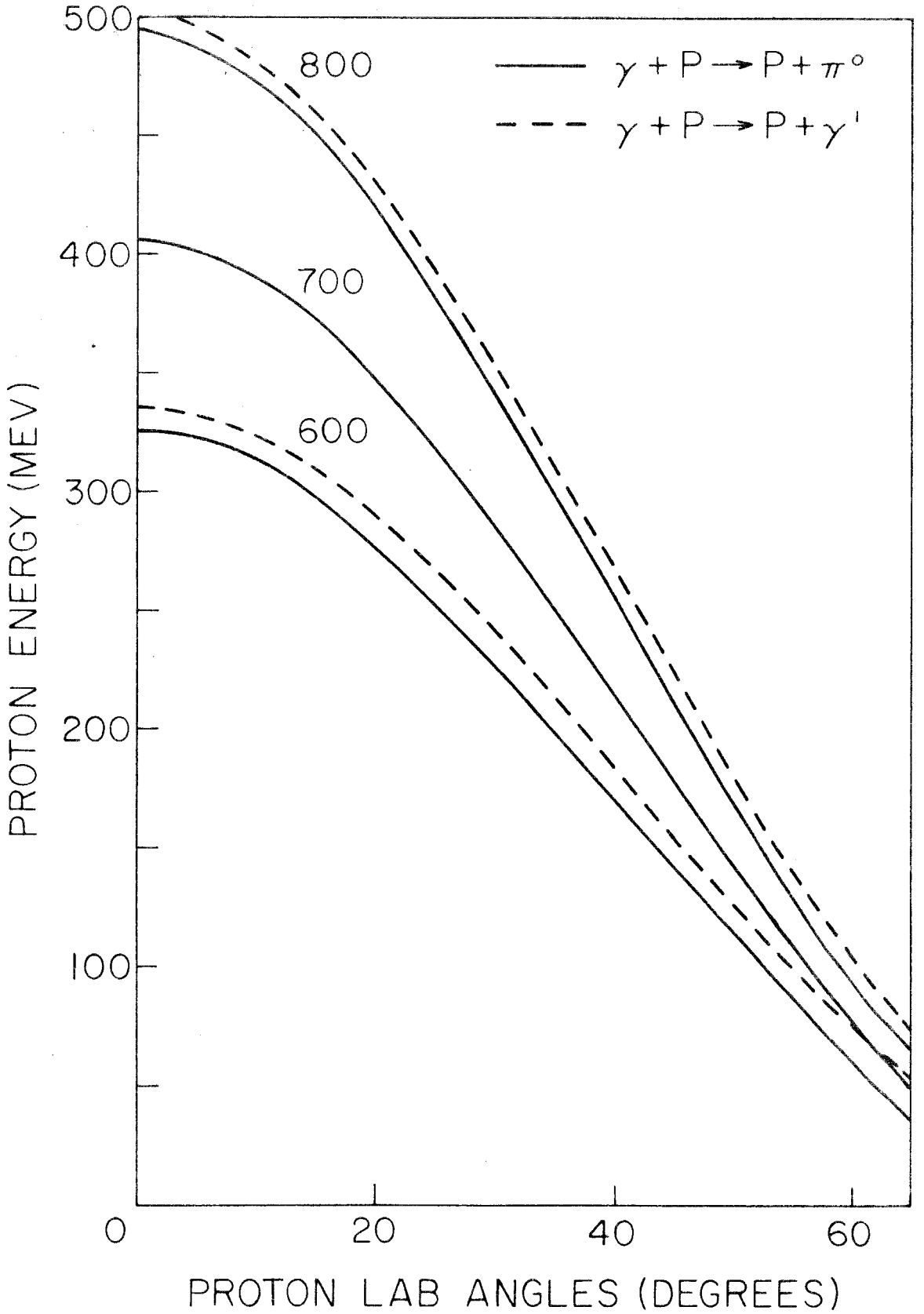
500
400
300
200
100
0
20
40
60
800
700
600
γ + P → P + π°
γ + P → P + γ'
PROTON ENERGY (MEV)
PROTON LAB ANGLES (DEGREES)

in the angular resolution of the telescope, which at large proton angles mainly determines the photon energy resolution. Since the telescope photon energy resolution function extends to energies above E_o, a further spreading due to scattering could be a source of error. However, calculation shows this effect to be small.

Two sources of error ascribable to electronic equipment have been examined. The first is dead time loss and the second is accidental coincidences.

Dead time losses consist of losses due to accidental vetoing of true events and can be caused by either the fast veto operated by counter 5 or the slow veto operated by the 23 coincidence. Using a dead time of 5×10^{-8} seconds for the fast and 3×10^{-7} seconds for the slow veto, the dead time loss in the most unfavorable case is found to be less than a per cent and is ignored. The counting rates are estimated on the basis of a uniform beam of 20 milliseconds duration. Since the #5 counting rate was not monitored, it was estimated from the #4 rate, since gains and biasses were approximately the same.

Accidental coincidences were monitored by counting 24(-5) coincidences in delayed coincidence with #1. This arrangement does not give an accidental correction directly, but does monitor about half the events which contribute to the measured proton counting rate. The 1*24(-5) rate was, in the worst cases, only about a per cent of the 124(-5) rate and this correction has also been ignored.

2. Cross-Section Calculation

When a "true" counting rate has been obtained from the data, it must then be converted into a cross-section to be of any real interest. The following is an expression for the differential counting rate in terms of the desired cross-section and other measurable and calculable quantities:

$$dN = \frac{d\sigma}{d\Omega'} \frac{d\Omega'}{d\Omega} d\Omega \, N(k)\, dk \, n(\tilde{r}) \frac{\rho N_0}{A} d^3\tilde{r}$$

where $\frac{d\sigma}{d\Omega'}$ = differential cross-section in cm system

$\frac{d\Omega'}{d\Omega}$ = solid angle transformation from cm to laboratory system at constant k

$d\Omega$ = differential laboratory solid angle

$\frac{\rho N_0}{A}$ = target nuclei per cm^3

$N(k)dk \times n(\tilde{r}) \frac{\rho N_0}{A} d^3\tilde{r}$ = number of photons/BIP at k in dk passing through $d^3\tilde{r}$ multiplied by target nuclei per cm^2 in $d^3\tilde{r}$. $n(\tilde{r})$ is the beam intensity distribution function discussed in Section II.

dN is the number of protons emitted into $d\Omega$ by photons of energy k in dk which strike target nucleons at $\tilde{r}$ in $d^3\tilde{r}$. To obtain the total counting rate a multiple integral over all variables must be computed. The quantity measured by the experiment is an average of the cross-section over the angular and energy ranges defined by the target-telescope system. If by $\frac{d\sigma}{d\Omega'}$ we now mean this average value, we may write

$$\frac{N}{BIP} = \frac{d\sigma}{d\Omega'}\int d^3\tilde{r}\int d\Omega\int dk\ \frac{d\Omega'}{d\Omega}\ \frac{U}{E_o}\ \frac{B(k,E_o)}{k}\ n(\tilde{r})\ \frac{\rho N_o}{A}$$

or $N/BIP = K\ \frac{d\sigma}{d\Omega'}$ where K represents the multiple integral. This integral may often be simplified. When the finite size of the target is unimportant the integral over the target volume may be carried out separately:

$$\int d^3\tilde{r}\ n(\tilde{r}) = \bar{\ell} \equiv \text{effective target length}$$

If $\frac{d\Omega'}{d\Omega}$ and $B(k, E_o)$ don't vary appreciably over the region of integration, the rest of the integral may be evaluated approximately, giving

$$K = \frac{d\Omega'}{d\Omega}\ \frac{U}{E_o}\ \frac{B(k,E_o)}{k}\ \frac{\rho N_o}{A}\ \bar{\ell}\ \Delta\Omega\ \Delta k$$

where Δk is given by $\Delta k \equiv \left.\frac{\partial k}{\partial T}\right|_\theta \frac{dT}{dR}\ \Delta R$

This approximation is quite satisfactory at forward proton angles (20^o to 40^o). At angles greater than 40^o, however, these conditions are not satisfied and the multiple integral must be done more carefully. At large angles the principal contributor to the broad photon resolution is the angular resolution of the system. Since the target is longer (3") than the width of the defining counter in the telescope, position of the target nucleon in the target becomes an important factor in determining photon energy resolution, and the integration over the target is no longer trivial. In addition, for low energy protons, the energy loss in travelling through the liquid hydrogen

varies appreciably over the target and should be taken into account.

As this is a rather complicated integral, a code has been developed by M. Ernstene and the author to enable the CIT Datatron digital computer to evaluate it. A brief description of the method may be found in Appendix A.

IV. RESULTS AND ERRORS

Sources of error have been classified into three groups according to the way in which they affect the results of the experiment. Below are listed the groups, the members of each group, and the estimated standard deviation due to each member.

I. Errors which vary randomly from point to point.

1. Counting statistics: 5°/o to 7°/o.
2. Uncertainty in separating proton peak from meson peak: 2°/o.
3. Variations in E_o, P, T, not taken into account by the periodic monitoring: 1°/o.

II. Errors which vary smoothly from point to point.

1. Nuclear absorption: 0°/o to 5°/o. (5°/o of the correction).
2. Pion pairs: 0°/o to 14°/o (25°/o of the correction).
3. Uncertainty in ΔR: 1.5°/o.
4. Uncertainty in range: 1.5°/o.
5. Uncertainty in $\Delta\Omega$: 1.5°/o.
6. Neglect of Compton scattering: < -3°/o (not included in calculating errors).

III. Errors which are constant for all points.

1. Beam calibration: < 3°/o.

Table 5 presents the cross-section values obtained in the experiment with their Type I and Type II errors and pair and absorption corrections. Figures 11 to 15 plot this data as excitation functions for fixed proton laboratory angle. Also shown are the photon energy resolution functions for k = 700 mev. Table 6

Table 5

Column 1: Point number.

Column 2: Proton laboratory angle, degrees.

Column 3: Mean photon energy, mev.

Column 4: Differential cross-section, units of 10^{-30} cm^2/ster.

Column 5: Type I error, per cent.

Column 6: Type II error, per cent.

Column 7: Combined Type I and Type II errors, per cent.

Column 8: Pair correction factor. Multiplying the cross-section of Column 4 by this quantity gives the cross-section which would be obtained if no pair correction were made.

Column 9: Absorption correction factor. The measured counting rate is multiplied by this factor to give the counting rate corrected for nuclear absorption.

Table 5

No.	θ_p	k	$d\sigma/d\Omega$	Type I	Type II	I+II	Pair	Abs.
1	19	599	2.35	9.4	10.2	13.9	1.38	1.59
2	21	613	2.28	10.6	10.8	15.1	1.41	1.59
3	19	702	2.37	8.5	14.2	16.5	1.54	1.98
4	19	804	3.07	7.9	11.6	14.0	1.41	2.48
5	30	600	3.52	7.3	4.9	8.8	1.15	1.41
6	30	709	4.19	5.8	4.2	7.2	1.08	1.81
7	30	765	3.96	5.6	4.1	6.9	1.00	1.64
8	30	793	3.72	5.5	4.6	7.2	1.06	1.89
9	40	601	3.50	5.6	2.8	6.3	1.00	1.24
10	40	699	4.50	5.6	3.0	6.4	1.01	1.35
11	40	795	3.90	5.7	3.6	6.8	1.07	1.49
12	50	600	2.91	5.8	2.7	6.4	1.00	1.12
13	50	695	3.92	5.9	2.7	6.5	1.00	1.16
14	50	795	3.66	7.0	2.8	7.5	1.00	1.23
15	60	600	2.16	7.2	2.6	7.7	1.00	1.05
16	60	700	2.30	7.0	2.6	7.5	1.00	1.07
17	60	800	2.11	7.2	2.6	7.7	1.00	1.09

Figures 11 to 15

Excitation functions. Differential cross-section is plotted against photon energy for proton laboratory angles of 19°, 30°, 40°, 50°, and 60°. Also indicated in each figure is an estimated photon energy resolution function for the $k = 700$ mev point. For a given proton angle, the resolution function will be slightly narrower at $k = 600$ and slightly broader at $k = 800$ mev.

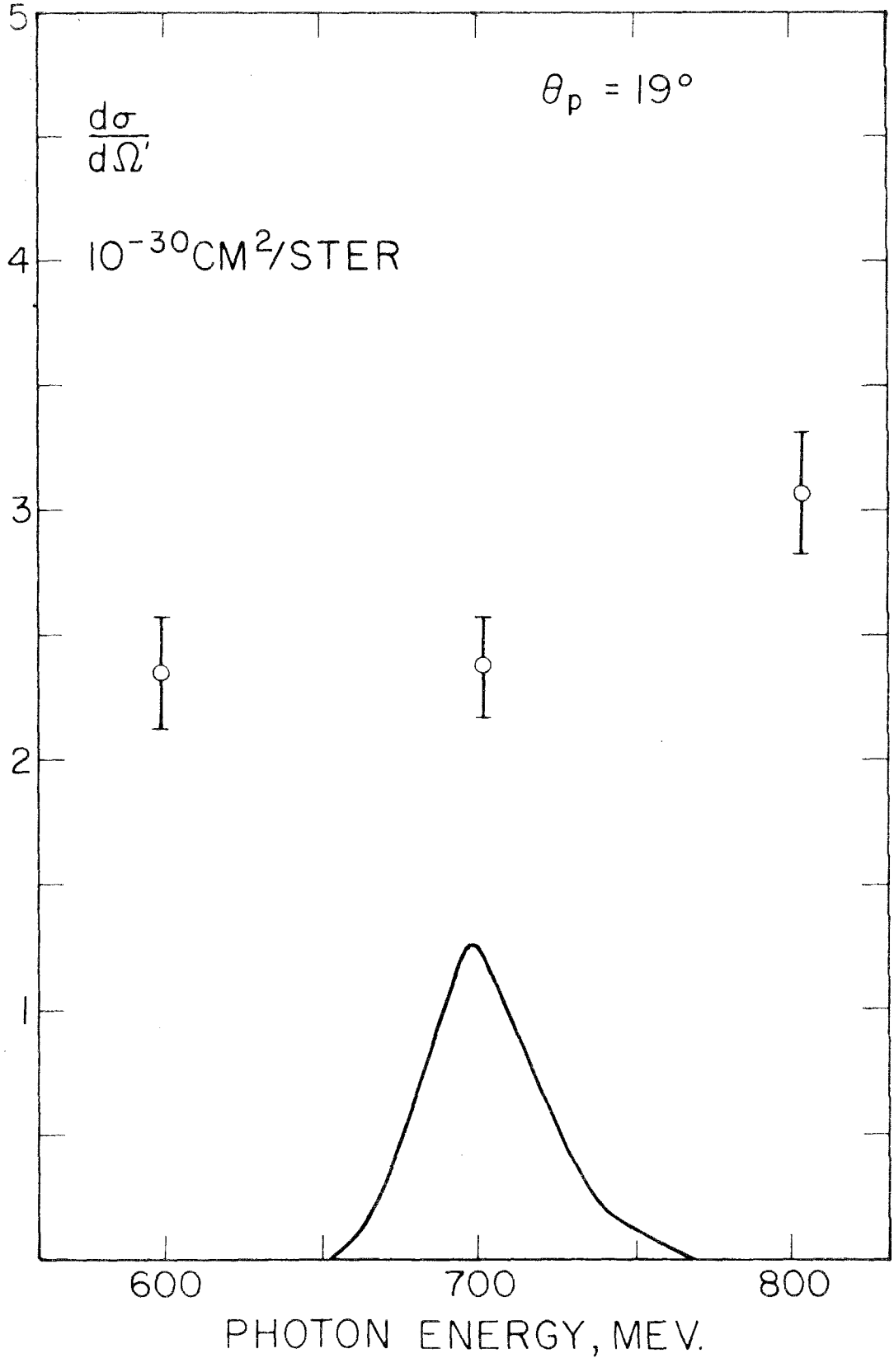
5
4
3
2
1
$\theta_p = 19°$
$\frac{d\sigma}{d\Omega'}$
$10^{-30} CM^2/STER$
600
700
800
PHOTON ENERGY, MEV.

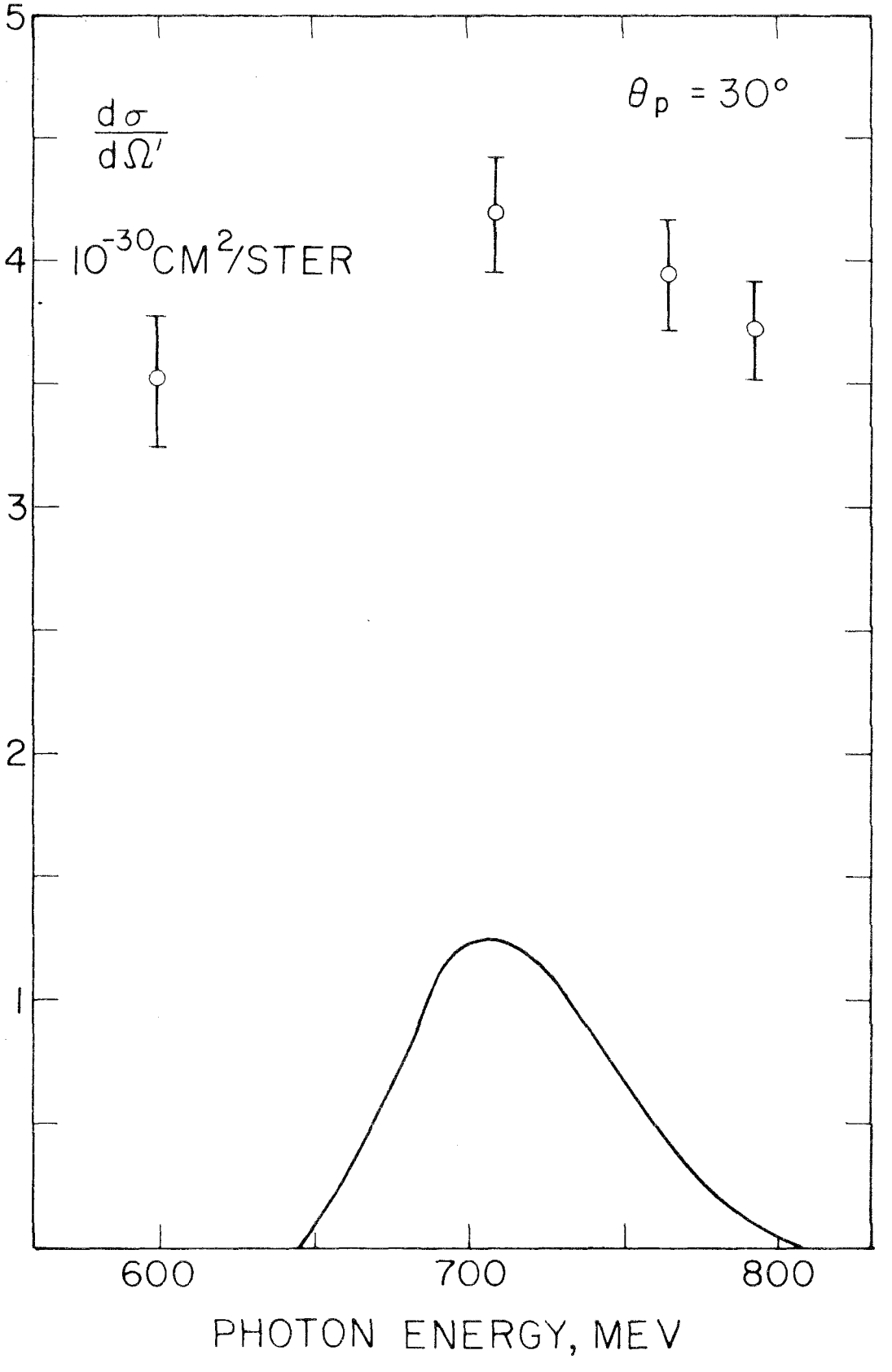
5
4
3
2
1
$\frac{d\sigma}{d\Omega'}$
10^{-30}CM^2/STER
$\theta_p = 30°$
600
700
800
PHOTON ENERGY, MEV

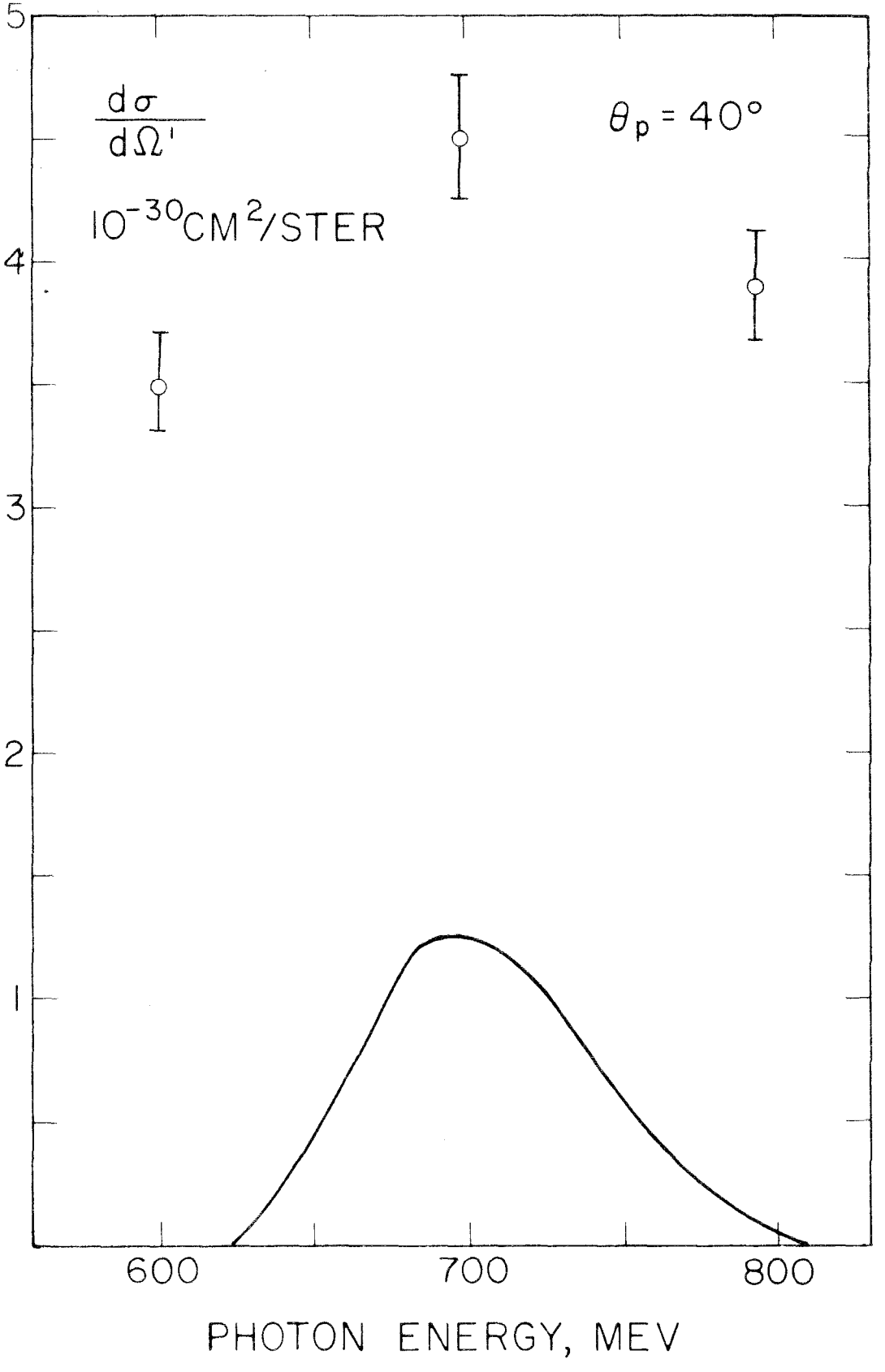
5
4
3
2
1
$\frac{d\sigma}{d\Omega'}$
10^{-30}CM^2/STER
$\theta_p = 40°$
600
700
800
PHOTON ENERGY, MEV

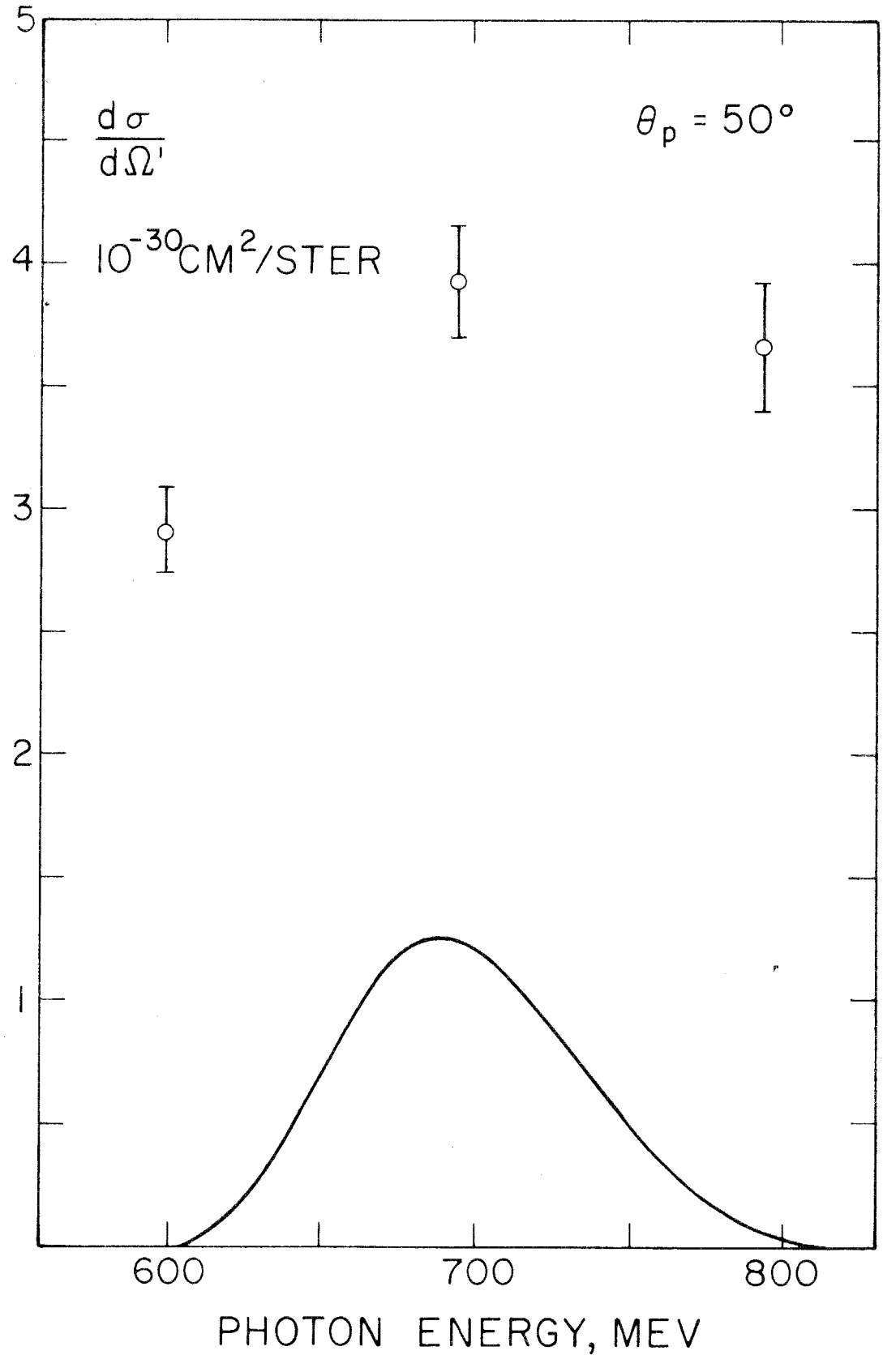
5
4
3
2
1
$\frac{d\sigma}{d\Omega'}$
10^{-30}CM^2/STER
$\theta_p = 50°$
600
700
800
PHOTON ENERGY, MEV

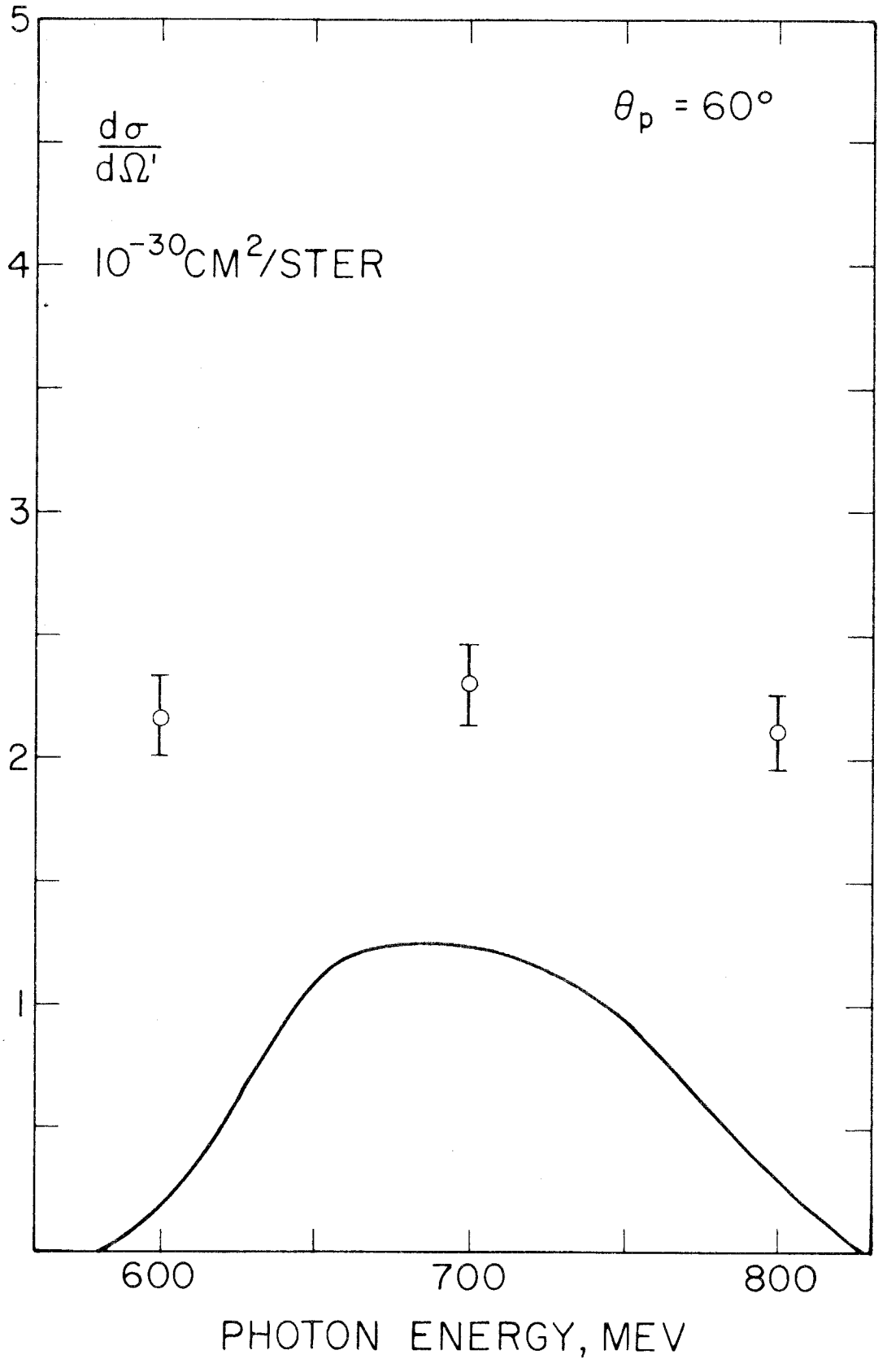
5
4
3
2
1
$\frac{d\sigma}{d\Omega'}$
$10^{-30} CM^2/STER$
$\theta_p = 60°$
600
700
800
PHOTON ENERGY, MEV

Table 6

Cross-sections for angular distributions.

Column 1: Mean photon energy, mev.

Column 2: Pion angle in center-of-momentum system, degrees.

Column 3: Differential cross-section, 10^{-30} cm^2/ster.

Column 4: Type I error, 10^{-30} cm^2/ster.

Column 5: Combined Type I and Type II error, 10^{-30} cm^2/ster.

Table 6

k	$\theta_{\pi'}$	$d\sigma/d\Omega'$	Type I	I + II
600	138	2.24	$\pm$.16	$\pm$.29
	115	3.52	.26	.31
	93	3.50	.20	.22
	72	2.91	.17	.19
	52	2.16	.16	.17
700	138	2.37	.20	.39
	114	4.16	.24	.30
	92	4.50	.25	.28
	72	3.91	.23	.25
	52	2.30	.16	.17
800	137	3.02	.24	.42
	113	3.67	.20	.26
	92	3.86	.22	.26
	72	3.65	.26	.27
	52	2.11	.15	.16

presents the cross-sections used in generating angular distributions. Small interpolations were necessary to obtain cross-sections at the desired energies. The measurements at 19^{o} and 21^{o} near k = 600 mev have been combined. Figures 16 to 18 exhibit the desired angular distributions. Through a least squares analysis, coded for the Datatron by J. I. Vette and W. Wales, the data of Table 6 have been used to determine angular distribution functions of the form: $A + B \cos\theta + C \cos^2\theta$. At k = 700 and 800 mev, a constraint had to be added to force the angular distribution function to be non-negative at all angles. This was done by introducing a very small cross-section at zero degrees. In the pion momentum range involved it would be reasonable to expect angular momenta of $\ell > 1$ to be present, but the form assuming only $\ell = 0, 1$ was used since 1) it gives a satisfactory fit to the data, and 2) the data are not sufficiently detailed to provide a good determination of higher order terms.

Table 7 exhibits the A, B, and C coefficients (in units of 10^{-30} cm^2/ster) as well as the total cross section $\sigma_T = 4\pi(A+\frac{C}{3})$ (units of 10^{-30} cm^2).

Table 7

k	A	B	C	σ_T
600	3.47 ± .16	-.55 ± .21	-2.70 ± .53	32.2 ± 1.4
700	4.31 ± .14	-.60 ± .24	-3.70 ± .29	38.7 ± 1.5
800	3.88 ± .14	-.87 ± .25	-3.00 ± .29	36.2 ± 1.5

Figures 19 to 21 present both the angular distributions of this experiment and those of Vette (10) at nearby energies. In

Figures 16 to 18

Angular distributions at k = 600, 700 and 800 mev. Errors on points are combined Type I and Type II. Curves are least squares fits of the form $A + B \cos\theta + C \cos^2\theta$.

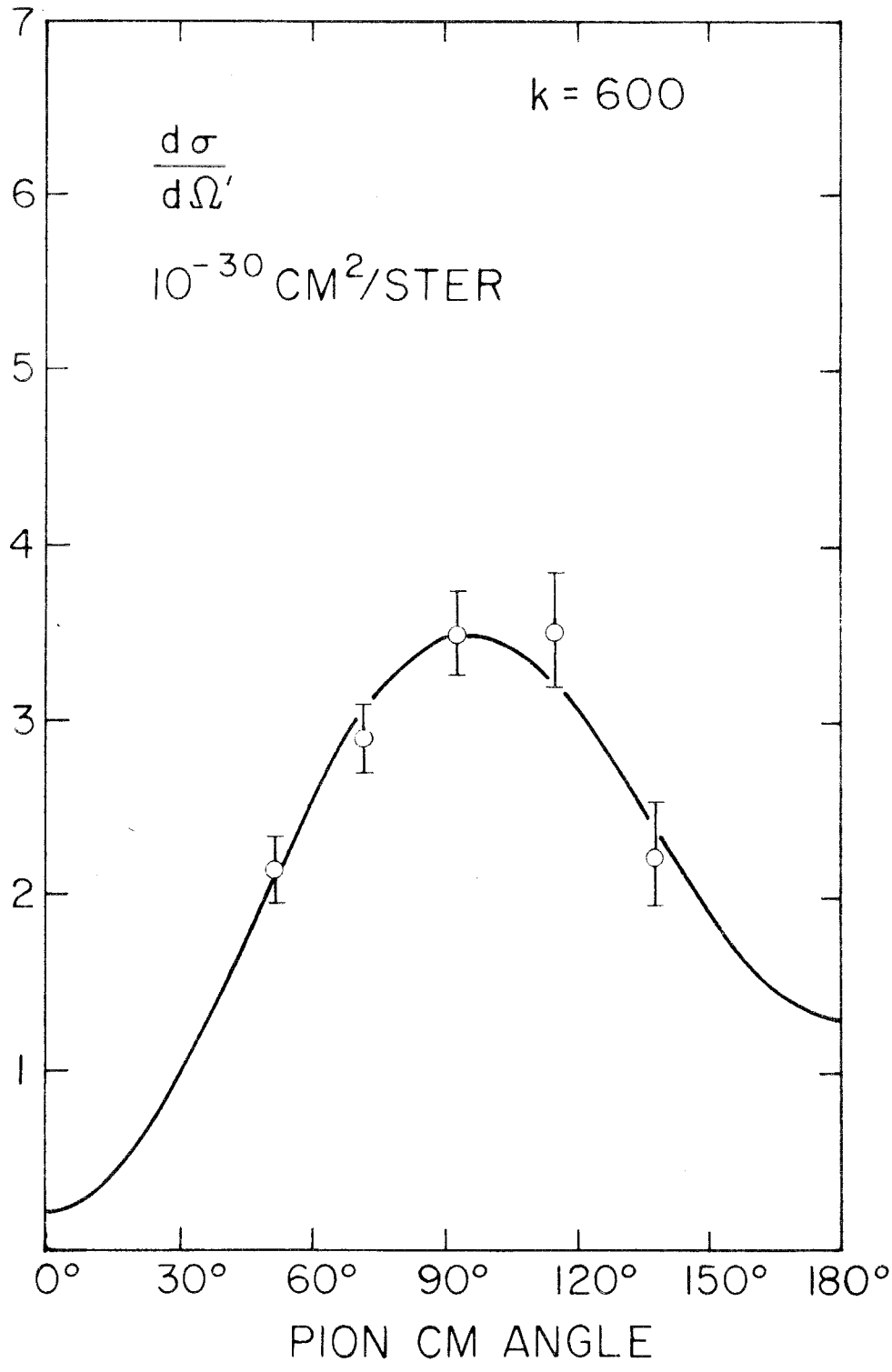
k = 600
dσ/dΩ'
10⁻³⁰ CM²/STER
7
6
5
4
3
2
1
0°
30°
60°
90°
120°
150°
180°
PION CM ANGLE

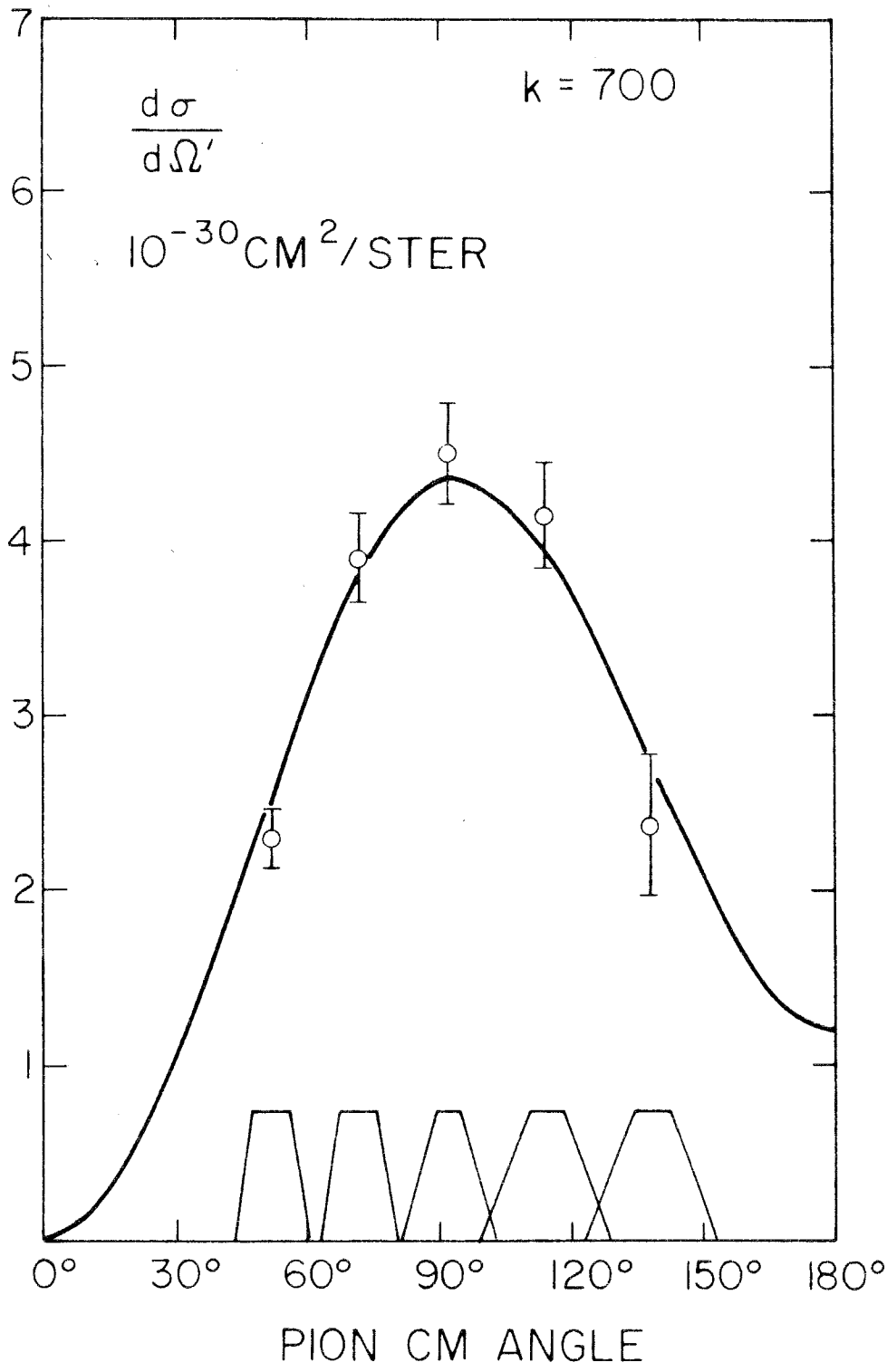
k = 700
dσ/dΩ'
10^-30 CM^2/STER
7
6
5
4
3
2
1
0°
30°
60°
90°
120°
150°
180°
PION CM ANGLE

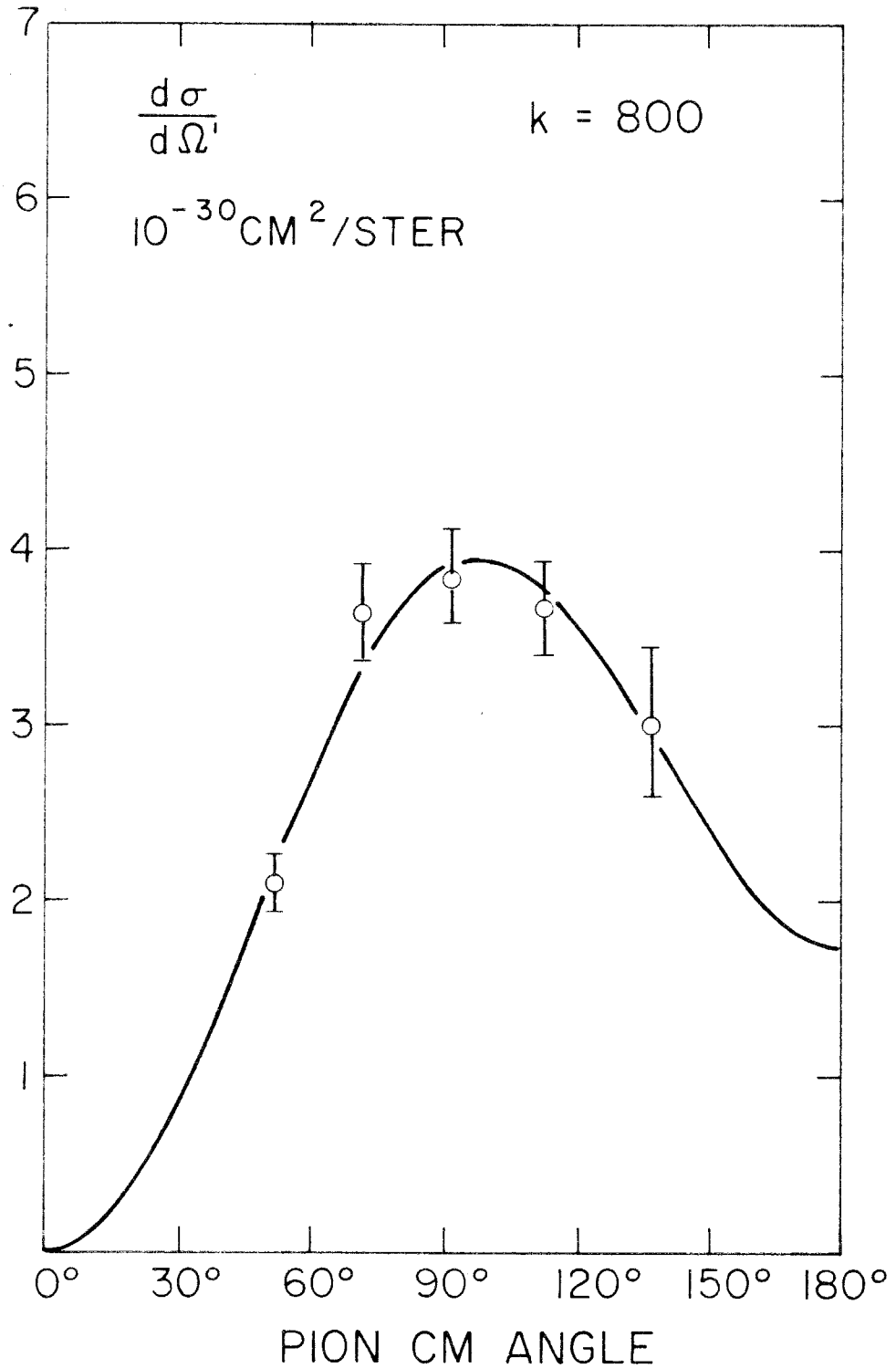
7
6
5
4
3
2
1
dσ/dΩ'
k = 800
10^-30 CM^2/STER
0°
30°
60°
90°
120°
150°
180°
PION CM ANGLE

Figures 19 to 21

Angular distribution data of this experiment plotted with that of Vette (10) at nearby energies.

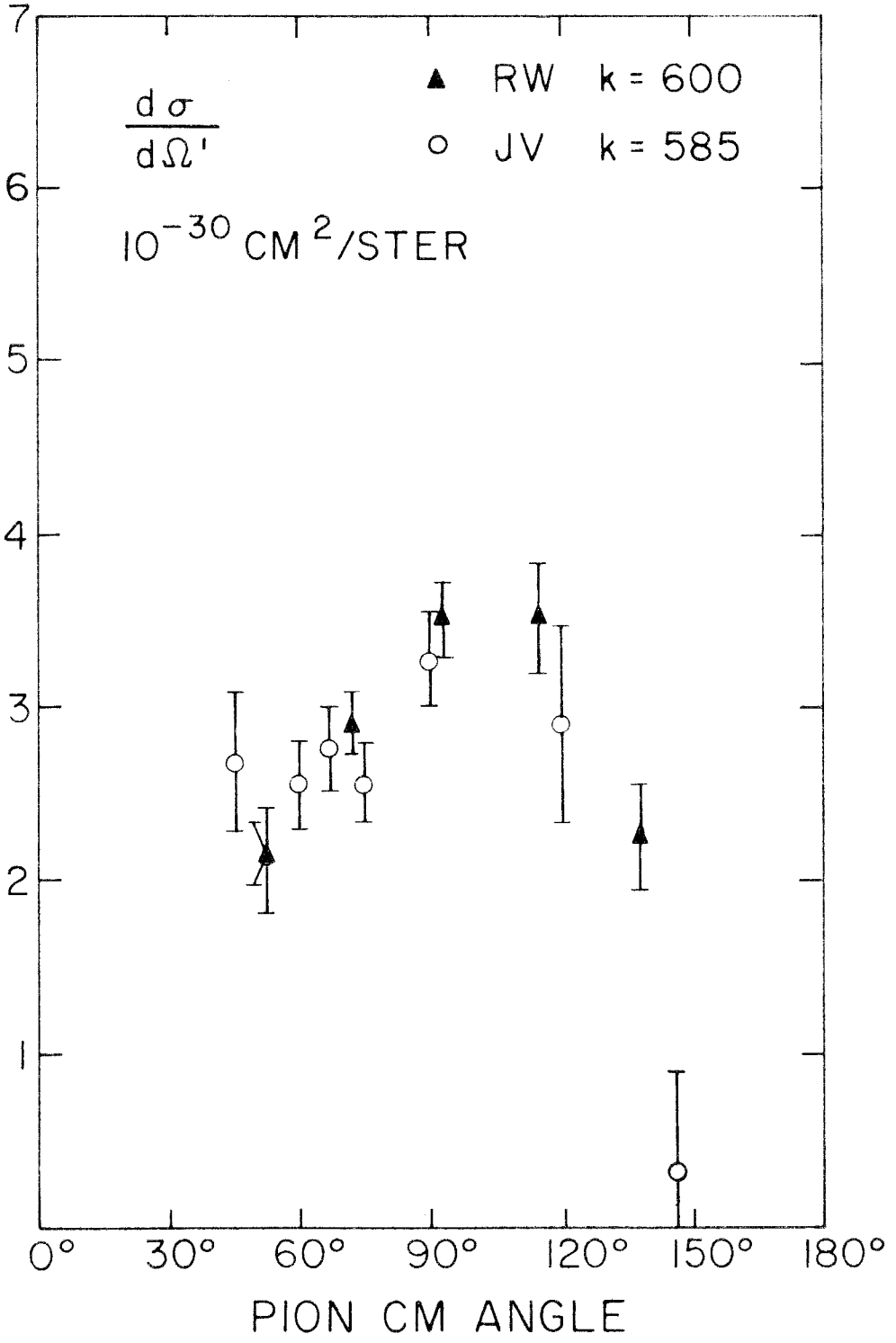
RW k = 600
JV k = 585
dσ/dΩ'
10^-30 CM^2/STER
7
6
5
4
3
2
1
0°
30°
60°
90°
120°
150°
180°
PION CM ANGLE

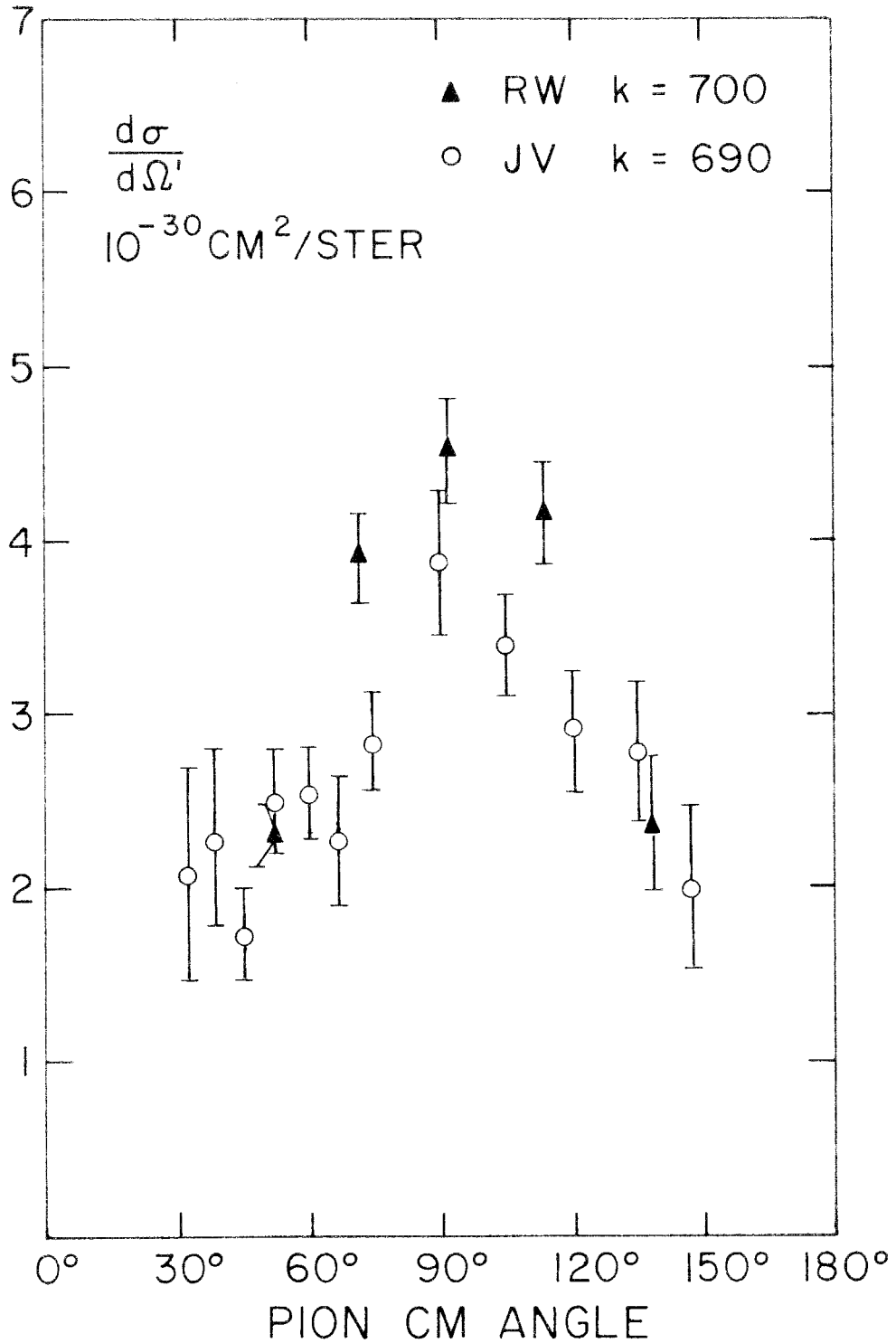
RW k = 700
JV k = 690
dσ/dΩ'
10^-30 CM^2/STER
7
6
5
4
3
2
1
0°
30°
60°
90°
120°
150°
180°
PION CM ANGLE

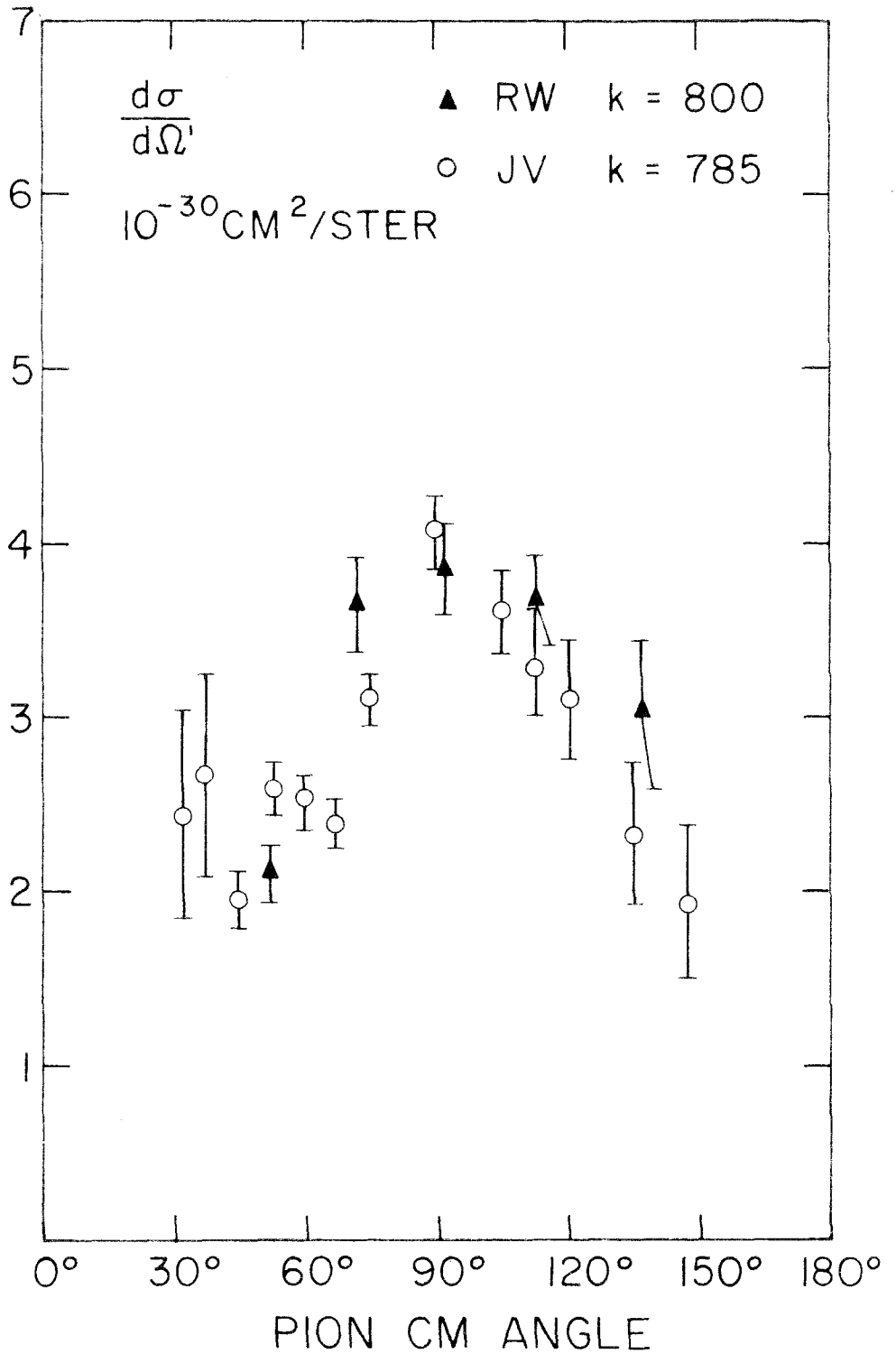
dσ/dΩ'
10^-30 CM^2/STER
▲ RW k = 800
○ JV k = 785
7
6
5
4
3
2
1
0°
30°
60°
90°
120°
150°
180°
PION CM ANGLE

general, the agreement is fairly satisfactory; no serious discrepancies are found in the 600 mev and 800 mev angular distributions although the results of this experiment tend to be somewhat higher. The worst disagreement seems to be between pion angles of 60^{o} and 120^{o} at k = 700 mev, where the results of this experiment are considerably larger. Unfortunately, the points of this experiment have not been re-run as much as would be desirable; the point at 92^{o} was determined from one set of full target runs and one set of empty target runs. The 72^{o} and 114^{o} points are slightly better; the 72^{o} point is based on two sets of runs and the 114^{o} point is reinforced somewhat by the measurement at the same angle but with k = 765 (see Figure 12).

In four cases, cross-sections were measured at widely separated times, between which the telescope was dis-assembled and the electronics used in another experiment. These points were: $\theta_p = 19^{o}$, k = 600; $\theta_p = 40^{o}$, k = 600; $\theta_p = 40^{o}$, k = 800; $\theta_p = 30^{o}$, k = 800. In the first three cases, the two measurements gave results which agreed well within statistics. The 30^{o}, 800 mev point was suspiciously large originally and was repeated for this reason. Two new measurements gave consistently lower results and were accepted; the old data were discarded. This success in reproducing cross-sections provides a certain amount of confidence in the rest of the measurements. In addition to these 3 points, 7 others are based on two sets of runs taken several days apart, all of which agree within statistics.

It is difficult to account for the discrepancy in the 700 mev angular distributions. It occurs in the region where it is easiest

to count protons: estimated pair contamination is small, absorption corrections are moderate, proton energies are high enough so scattering isn't important, and counting rates are good. Two possible sources of error are: 1) failure of beam monitoring equipment, and 2) changes in characteristics of target (icing). Little is known about these--they have never been shown to cause trouble.

V. INTERPRETATION

As mentioned in the introduction, a theoretical interpretation of the data is not possible at this time. Methods which were successful at lower energies are not applicable here, partly for lack of a suitable theory or model and partly for lack of data such as pion-nucleon scattering phase shifts and charged pion photoproduction data with which the data presented here might be correlated.

A few remarks might be made on the general behavior of the angular distributions in the 600 to 800 mev range. As can be seen from Figures 16 to 18, they are qualitatively like the angular distributions at lower energies, where the data can be fit quite well with $(5 - 3 \cos^2\theta)$, the angular distribution given by magnetic dipole absorption and $j = 3/2$ final state (24). They differ in that the quantity $-A/C$, which is 1.6 at low energies, is roughly 1.25 from 600 to 800 mev. In both regions, the coefficient B is small, crossing over from positive to negative somewhere around 500 mev.

Lacking the means of making a more detailed analysis, it was felt that it might be interesting to examine the energy dependence of the total cross-section for an indication of interference between states of isotopic spin 3/2 and 1/2. The resonance at $k = 330$ mev is due almost entirely to a $T = 3/2$ state. Since this corresponds to a $T = 3/2$ resonance in pion-nucleon scattering, perhaps the $T = 1/2$ peak in scattering at a pion energy of 800 mev (9) has a counterpart in photoproduction which leads to an interference term.

The photoproduction amplitude can be written as the sum of two pure isotopic spin states: $\Psi = \Psi_3 (T = 3/2) + \Psi_1 (T = 1/2)$. To make a simple model, represent each state with a resonant term of the form $\Psi_j = \frac{a_j}{E - E_j + i\gamma_j}$. It is realized that this is a non-relativistic expression and not entirely applicable here; it is used because of its simplicity. Then

$$\Psi = \frac{a_3}{E - E_3 + i\gamma_3} + \frac{a_1}{E - E_1 + i\gamma_1}$$

and

$$\sigma = \frac{|a_3|^2}{(E-E_3)^2 + \gamma_3^2} + \frac{|a_1|^2}{(E-E_1)^2 + \gamma_1^2} + 2\,\mathrm{Re}\left[\frac{a_3^* a_1}{(E - E_3 + i\gamma_3)(E - E_1 + i\gamma_1)}\right]$$

From the (3, 3) resonance we determine $E_3 = 330$ mev, $\gamma_3 = 71$ mev, and $\left(\frac{a_3}{\gamma_3}\right)^2 = 270\ \mu$b (24). From the T = 1/2 scattering data we decide upon a resonance at $T_\pi = 800$ mev with a width of 300 mev (9). Using the easily derivable relation that for equal center of momentum energy of the pion-nucleon system, $k = T_\pi + 150$ mev, we choose $E_1 = 950$ mev and $\gamma_1 = 300$ mev. This leaves two parameters free: a_1 and the relative phase of a_1 and a_3. Using these, an attempt was made to fit the experimental data. As can be seen in Figure 22, which shows an attempt using no interference term, the agreement is not striking. Just as good a fit can be obtained without an interference term as with one. The minimum at 600 mev is much too sharp to be produced by such a broad resonance. Of course, if E_1 and γ_1 are also considered to be variable parameters, a better fit can be made.

Thus, without further information, this two resonance idea seems not to be very instructive. It is possible that the

Figure 22

Total cross-section results of this experiment plotted with those of Vette (10). Curve is attempt to fit data using two resonant terms, but with no interference between the resonances.

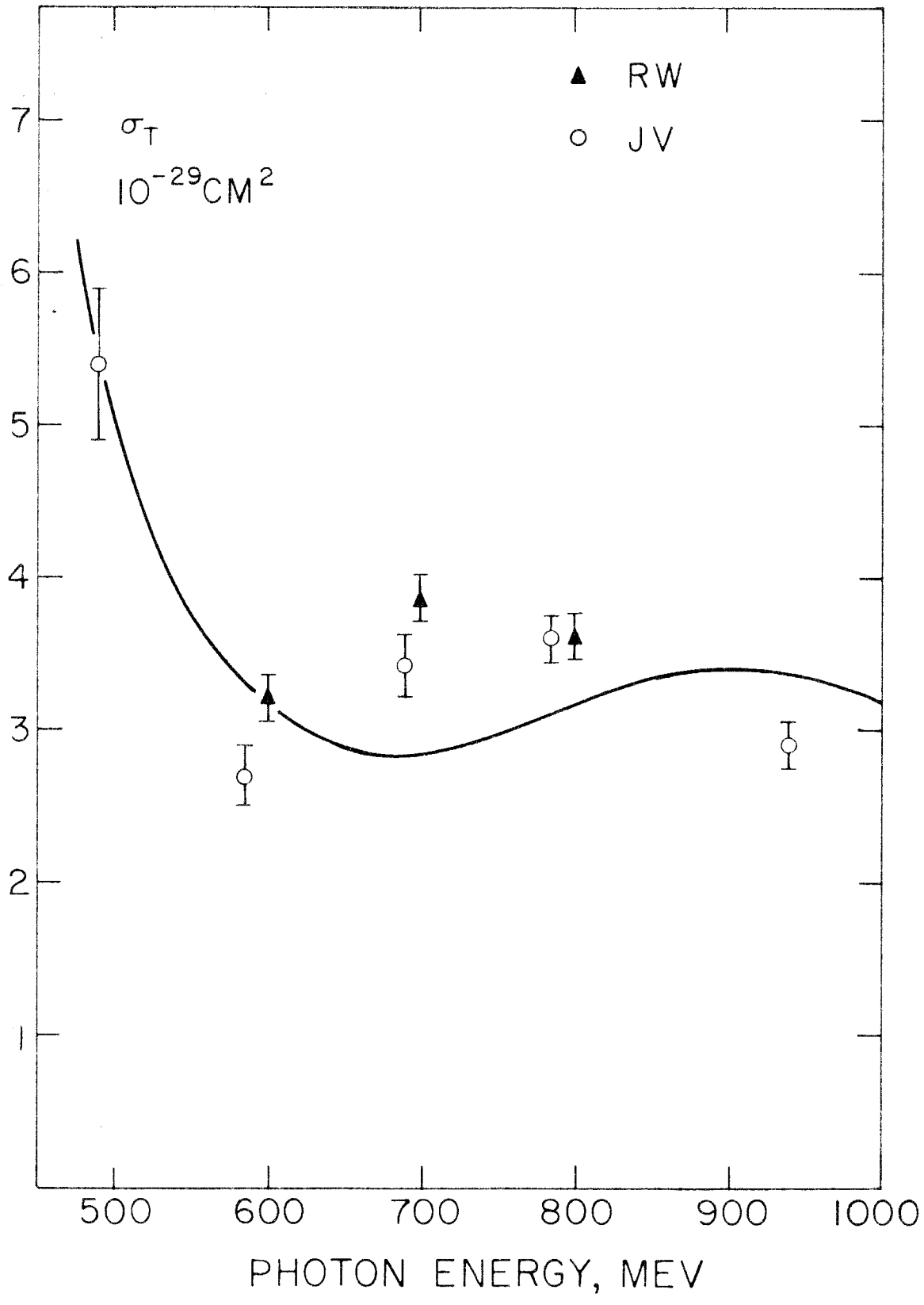
RW
JV
σ_T
$10^{-29}CM^2$
7
6
5
4
3
2
1
500
600
700
800
900
1000
PHOTON ENERGY, MEV

behavior of the total cross-section in this energy region is related to competition with other processes such as multiple pion production, and for this reason is not explained by such a simple model.

VI. SUGGESTIONS

There is clearly a need for a good deal more work in determining accurately the π^o photoproduction cross-section above 500 mev. The first task should be to clear up the discrepancy in the 700 mev angular distribution which exists between magnetic spectrometer and counter telescope measurements of the cross-section. When this has been done, more precise experiments can be planned. Four main points come to mind when one considers how the present experiment could be improved.

The first concerns reduction of pair contamination. This is important since the correction for the contamination is a major source of error. According to the model used here, pair contamination is important only at the forward proton angles. At these angles the photon energy resolution is fairly narrow, so E_o could be reduced substantially without cutting into the resolution, thus reducing the pair contamination to a few per cent. In addition, further checks on the adequacy of the model used should be made and the problem of the value of the parameter "a" cleared up.

The second concerns photon energy resolution. As has been shown, the photon energy resolution function at the larger proton angles is quite broad; at 60^o and k = 800 mev, it is 200 mev wide at half height and would be wider if the bremsstrahlung limit didn't cut it off. For a reasonably precise experiment this width should be kept under 100 mev. Since the majority of the width at large proton angles is contributed by the angular resolution, a narrower angular resolution is called for; at 60^o and k = 800 mev

a width at half height of 3° would be about right. In addition, somewhat better angular resolution for its own sake would be worthwhile at the forward proton angles; the resolution used in this experiment for the $\theta_{\pi}^{*} = 92^{\circ}$, k = 700 mev point should suffice for all but the most precise experiments.

The third point concerns the absorption correction. It would be highly advantageous to have direct measurements of the absorption of protons in copper, rather than having to rely on a calculated value. Such measurements could be made in a reasonable length of time using existing magnetic spectrometers.

The fourth concerns extension of the angular region covered. This would be a very desirable improvement since all the data of this experiment were taken between 52° and 138° in the pion cm system. For a given photon energy, the problem at forward proton angles is mainly an electronic one, caused by greatly increased individual counting rates, due in large part to electrons. This can be alleviated by any combination of three things: 1) better electronic equipment, 2) reduced beam intensity, and 3) a cleaner target. It shouldn't be too difficult to operate as far forward as 14° or 15°. A measurement at 0° will have to be left to a magnetic spectrometer experiment. At larger proton angles, the problem is one of proton range and photon energy resolution produced by angular resolution. Here again, nothing basic need be done to work as far back as 70°--counters must be somewhat thinner and angular resolution narrowed. The main difficulty then would be the low counting rate.

APPENDIX A

In Section III it was seen that to convert counting rates to cross-sections, it is necessary to evaluate the following integral:

$$K = \int d^3\tilde{r} \int d\Omega \int dk \, \frac{d\Omega'}{d\Omega} \frac{U}{E_o} \frac{B(k, E_o)}{k} n(\tilde{r}) \frac{\rho N_o}{A}$$

This has been done as follows:

Define $$P(\tilde{r}) = \int d\Omega \int dk \, \frac{d\Omega'}{d\Omega} \frac{B(k, E_o)}{k}$$

Except for multiplicative constants this is the integral over the photon energy of the resolution function for the telescope with a target nucleon at $\tilde{r}$. $P(\tilde{r})$ is written as a power series in the target coordinates:

$$P(\tilde{r}) = a_o + a_1 y + a_2 z + a_3 y^2 + \cdots$$

The coordinate system used is: origin at center of target, z pointing downstream along the beam, x pointing up, and y chosen to make a right-handed system. The dependence of P on x is very small and is neglected. The coefficients in the expansion are determined by calculating $P(\tilde{r})$ at a number of points in the target.

$$P_o = a_o + a_1 y_o + a_2 z_o + \cdots$$

$$\vdots$$

$$P_n = a_o + a_1 y_n + a_2 z_n + \cdots$$

This can be expressed in matrix form as $P = Ra$ where, if n is the number of target points used, P is an n x 1 column matrix, R

is an n x n matrix, and a is an n x 1 column matrix. Then $a = R^{-1}P$. Now

$$K = \frac{U}{E_o}\frac{\rho N_o}{A}\int d^3\tilde{r}\, P(\tilde{r})\, n(\tilde{r})$$

$$K = \frac{U}{E_o}\frac{\rho N_o}{A}\left[a_o\int n(\tilde{r})d^3\tilde{r} + a_1\int y\, n(\tilde{r})d^3\tilde{r} + \cdots\right]$$

The integrals may be identified as the various moments of the beam distribution over the target and are grouped together to form a 1 x n row matrix: $M = (M_o\ M_1 \cdots M_n)$

Then $$\frac{K}{\frac{U}{E_o}\frac{\rho N_o}{A}} \equiv K' = Ma = MR^{-1}P = CP$$

where $C = MR^{-1}$ is a 1 x n row matrix. Thus the integration over the target is accomplished by taking a linear combination of the P_i's calculated at different points in the target.

The beam moments M_i are calculated numerically in a straightforward manner on the CIT Datatron. The target volume is divided into cells, a value of $n(\tilde{r})$ calculated and assigned to each cell and the appropriate quantities (n, nz, ny^2, etc.) summed over all the cells. When M has been calculated, $C = MR^{-1}$ can be found.

Next let us discuss the calculation of the P_i. Once the target point and the telescope parameters (range, ΔR, geometry) are determined, the corresponding rectangle in T, θ space may be determined. Then $k_{max} = k(T_{max}, \theta_{max})$ and $k_{min} = k(T_{min}, \theta_{min})$ are calculated and the region between divided into k-intervals.

For each k-interval, the following quantity is calculated:

$$I(k) = \frac{B(k,E_o)}{k}\int d\Omega \frac{d\Omega'}{d\Omega}$$

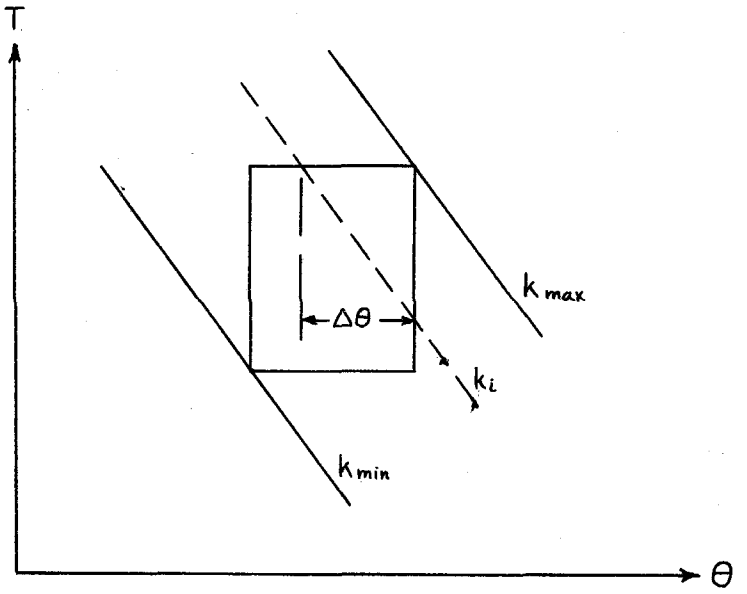

The first step is calculation of θ_- and θ_+, the values of θ where the appropriate k line enters and leaves the T, θ rectangle. The range $\Delta\theta = \theta_+ - \theta_-$ is then divided into intervals. For each interval, $\frac{d\Omega'}{d\Omega}(k,\theta_i)\sin\theta_i$ is calculated and multiplied by $(\Delta\phi)_i$ which is found by calculating the values of ϕ where a line of constant $\theta = \theta_i$ drawn from the target point in question intersects the boundaries of the defining counter. A Simpson's Rule Integration is then performed over $\Delta\theta$ to give $\int\int \frac{d\Omega'}{d\Omega}\sin\theta\, d\theta\, d\phi$. The result is multiplied by $2\pi\frac{B(k,E_o)}{k}$ to give I(k) which is printed out for each k to give the counter photon energy resolution function for that target point. I(k) is also multiplied by the appropriate C_j and stored. This process is repeated for each target point and at the end, the $C_jI_j(k)$ are added and a Simpson's Rule Integration over k performed

to give $\int dk \sum C_j I_j(k)$ which is the definition of K^1 except for an interchange in order of integration and summation.

To produce a total photon energy resolution function the already obtained result $\sum C_j I_j(k)$ is not very satisfactory since only enough target points are used to give a satisfactory expansion of $P(\tilde{r})$. This does not give a satsifactory expansion of $I(k)$, which varies much more rapidly over the target. Instead, to produce an approximate resolution function, another linear combination of the I_j, chosen to give a better indication of the variation of $I(k)$ over the target, is used.

In this experiment 11 target points were used, although at most of the telescope settings, fewer would have sufficed. This number was required to give an accurate expansion of $P(\tilde{r})$ at the most difficult point: $\theta_p = 60^o$, $k = 800$ mev.

REFERENCES

1. Panofsky, Steinberger, and Steller, Phys. Rev. 86, 180 (1952)
2. Silverman and Stearns, Phys. Rev., 88, 1225 (1952)
3. Goldschmidt-Clermont, Osborne, and Scott, Phys. Rev., 89, 329L (1953), Phys. Rev., 97, 188 (1955)
4. Walker, Oakley, and Tollestrup, Phys. Rev., 97, 1279 (1955)
5. Oakley and Walker, Phys. Rev., 97, 1283 (1955)
6. McDonald, Peterson, and Corson, Phys. Rev., 107, 577 (1957)
7. Watson, Keck, Tollestrup, and Walker, Phys. Rev., 101, 1159 (1956)
8. Chew and Low, Phys. Rev., 101, 1579 (1956)
9. Cool, Piccioni, and Clark, Phys. Rev., 103, 1082 (1956)
10. J. I. Vette, Ph.D. Thesis, Cal Tech (1958)
11. Tollestrup, Keck, and Worlock, Phys. Rev., 99, 220 (1955)
12. Walker, Teasdale, Peterson, and Vette, Phys. Rev., 99, 210 (1955)
13. R. Gomez, "Preliminary Calibration of the Beam Monitor of the Cal Tech Synchrotron," (1957), Unpublished
14. R. R. Wilson, Nuclear Instruments, 1, 101 (1957)
15. Donoho, Emery, and Walker, Private Communication
16. Rich and Madey, UCRL-2301 (1954)
17. Fernbach, Serber, and Taylor, Phys. Rev., 75, 1352 (1949)
18. M. L. Goldberger, Phys. Rev., 74, 1269 (1948)
19. B. Rossi, High Energy Particles, 347 (1952)
20. Millburn, Birnbaum, Crandall, and Schecter, Phys. Rev., 95, 1268 (1954)
21. M. Bloch, Ph.D. Thesis, Cal Tech (1958)

REFERENCES (Cont'd)

22. Auerbach, Bernardini, Filosofo, Hanson, Odian, and Yamagata, CERN Symposium Vol. II, 291 (1956)

23. J. Mathews, Ph. D. Thesis, Cal Tech (1957)

24. W. McDonald, Ph. D. Thesis, Cal Tech (1957)